Escola de Camins
Escola Tècnica Superior d'Enginyeria de Camins, Canals i Ports
UPC BARCELONATECH

3D numerical simulation of experiments on masonry arch bridges

Treball Final de MÀSTER

Treball realitzat per:
Ignacio Brunet Coll

Dirigit per:
Climent Molins Borrell

Màster en:
Enginyeria de Camins, Canals i Ports

Barcelona, 22 juny de 2016

Departament d'Enginyeria Civil i Ambiental

ACKNOWLEDGEMENTS

Foremost, I would like to thank my tutor, Professor Climent Molins for guidance, support and supervision. And also to my family who supported me economically and was always there to encourage me in difficult times.

Furthermore, I would also like to thank all the lecturers who participated during the classes of the Bachelor and Master in the School of Civil Engineering at the University Polytechnic of Catalonia for sharing their great knowledge.

ABSTRACT

Masonry arch bridges are one of the oldest civil engineering heritage preserved until today. Besides having great historical and engineering value, most are still functional and come to be approximately 60% of the total European masonry railway bridge stock.

Most of these structures have to withstand increased axle loads higher than the designed ones. Consequently, many masonry bridges are damaged and need to be refurbished and in worst cases replaced.

The Construction Engineering Department of the Polytechnic University of Catalonia carried out a real-scale masonry arch bridge aiming to improve the understanding of these types of structures. Since this experimental test, and based on previous studies of the same case of study, this dissertation has the objective to set up a three-dimensional numerical model to reproduce the same results obtained in the laboratory.

First, a current state of the art about these types of structures is presented including a brief description of the main structural elements and their typologies, the main characteristics of masonry and a brief history of the analysis of these structures, from its beginnings in the seventeenth century till the implementation of finite element method.

Moreover, the construction, material characterization and test instrumentation of the experimental test is described. The results are analysed and compared with previous analytical and numerical predictions.

Finally, a non-linear analysis of a new three-dimensional model including all the main structural elements and interactions between them through the use of interface elements is performed.

Key words: masonry bridges, structural nonlinear analysis, 3D FE model.

RESUMEN

Los puentes en arco de obra de fábrica son una de las formas de paso más antiguas que se conservan hoy en día. Además de tener gran valor patrimonial e ingenieril, la mayoría aún son funcionales y llegan a representar hasta el 60% del total de los puentes de ferrocarril en Europa.

La mayor parte de estas estructuras han visto aumentar considerablemente sus cargas en los últimos años. En consecuencia, muchos puentes de obra de fábrica se encuentran deteriorados y necesitan ser analizados y en el peor de los casos rehabilitados.

En el Departamento de Ingeniería de la Construcción de la Universidad Politécnica de Cataluña se llevó a cabo un ensayo de un puente en arco de obra de fábrica a escala real enfocado a la mejora del entendimiento del funcionamiento de este tipo de estructuras. A partir de este ensayo y de varios estudios previos del mismo, esta tesina tiene como principal objetivo realizar un modelo numérico tridimensional que permita reproducir los mismos resultados obtenidos en el laboratorio.

Primero, se presenta un estado actual del conocimiento detallado sobre este tipo de estructuras incluyendo una breve descripción de los principales elementos estructurales y sus principales tipologías, principales rasgos de la obra de fábrica como material y una breve historia del análisis de este tipo de estructuras, desde sus inicios en el siglo XVII hasta la actualidad con la implementación del método de los elementos finitos.

Después, se describe la construcción y ejecución del ensayo realizado en el laboratorio. Se analizan los resultados y se contrastan con diversos modelos numéricos que fueron realizados posteriormente.

Finalmente, se realiza un análisis no-lineal de un nuevo modelo tridimensional incluyendo todos los principales elementos estructurales y sus interacciones entre ellos por medio de elementos de interfaz.

Palabras clave: puentes en arco de obra de fábrica, análisis no lineal, modelo EF 3D.

CONTENTS

LIST OF FIGURES

LIST OF TABLES

1 INTRODUCTION AND OBJECTIVES

1.1 MASONRY ARCH BRIDGES

Masonry arch bridges are part of our heritage and form a substantial part of the widespread European infrastructure of roads and railway bridges. Up to 60% of the bridges of the European railway network follow this typology and around 85% of them are single span bridges.

Figure 1-1 Stari Most from Mostar (Bosnia and Herzegovina), Pont del Diable from Martorell (Spain) and Ponte Vecchio from Florence (Italy).

Most of them are more than 100 years old and are still in service despite their age and the significant changes in loading conditions since their construction. The design of these structures was based on empirical rules which were too conservative taking advantage to their shape which provides great resistance. Together with the durable material properties of masonry, this has resulted in structures with an inherent ability to withstand the applied loads and extreme weathering conditions.

To preserve our heritage and to utilize these bridges to their maximum capacity, understanding of arch bridges is vital. For this reason, a significant amount of experimental evidence on the structural response of masonry arch bridges has been done in the last decades.

Aiming at providing more experimental results useful for the validation of analytical and numerical tools, the Structural Technology Lab of the UPC tested up to failure two full-scale masonry arch bridges. One of them was a segmental arch bridge which has been studied in several dissertations mostly in numerical plane stress models.

1.2 OBJECTIVES

Taking advantage of previous works of the same case of study, the main objective of this thesis is to simulate numerically the structural behaviour of masonry arch bridges near collapse, its ultimate capacity and its collapse mechanism.

In more detail, this dissertation aims at the following:

(1) Literature review on the simulation of masonry arch bridges by 3D FE analysis, also from previous Master Thesis at the UPC.
(2) Collection and interpretation of the test data.
(3) Selection of the best approaches, type of FE and constitutive equation for both brick masonry and spandrels infill from those available in Diana software and generate a 3D FE model.
(4) Development of the analysis and sensitivity of the results to uncertain variables.
(5) Edition of the results and conclusions related to the accuracy of the simulation.

1.3 CONTENTS OF THIS DISSERTATION

This dissertation consists of 6 different chapters. The first one is about the introduction and objectives to be fulfilled within the thesis.

Chapter 2 presents a current state of the art about these types of structures. It includes a brief description of the main structural elements and their typologies, the main characteristics of masonry and a brief history of the analysis of these structures.

Chapter 3 continues with the description of the experimental test of the full-scale masonry arch bridge carried out by the Structural Technology Lab of the UPC. Geometry, construction procedure, test instrumentation and results are presented.

Chapter 4 includes previous analytical and numerical predictions of the same case of study. Most of this works are from previous Master Thesis at the UPC and also use the Diana software.

In Chapter 5 a non-linear analysis of a new three-dimensional model including all the main structural elements and interactions between them through the use of interface elements is performed.

Finally, the dissertation ends with chapter 6 where a discussion of the results is done and a guideline is presented for future research.

2 CURRENT STATE OF KNOWLEDGE

Chapter two starts introducing the basic and structural elements of masonry arch bridges. Moreover, shows the general behaviour of the structure under load and the interaction of the elements.

Finally, a brief history of approach analysis is presented.

2.1 PARTS OF THE MASONRY ARCH BRIDGE

A masonry arch bridge is composed for a large number of elements as it can be seen in Figure 2-1. First, in order to know the behaviour of masonry arch bridges is worth to point out to the principal elements and especially to the ones with a structural function.

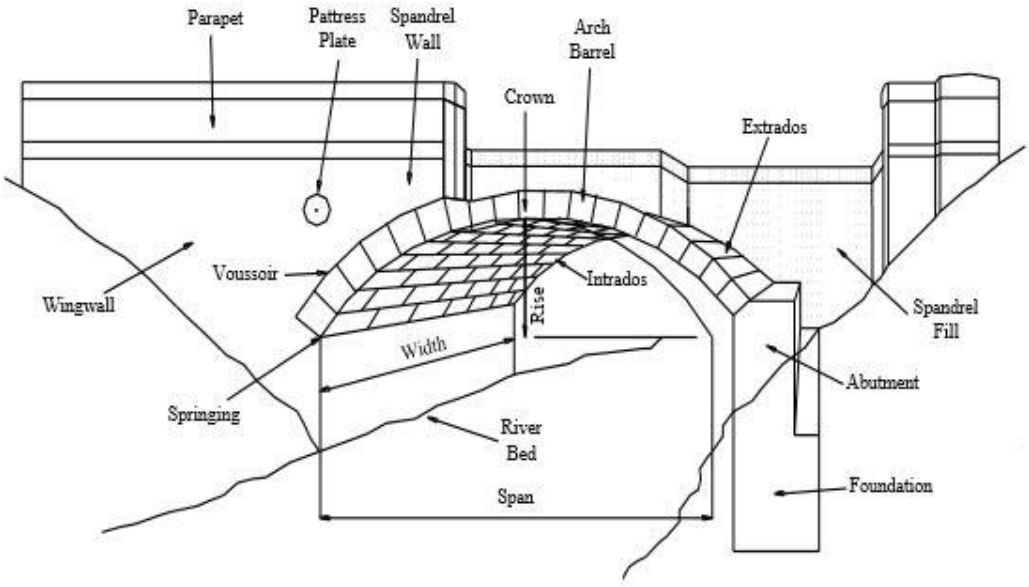

Figure 2-1 main elements of masonry arch bridge (Mckibbins, L. 2006).

The main structural element is the arch which as a curved structure is capable of supporting vertical loads across an opening and transferring these loads to piers or abutments. Furthermore, the fill, spandrel wall and abutments also have structural functions.

Masonry is the building of structures from individual units laid in and bound together by mortar. The common materials of masonry bridge construction are brick and building stone. The blocks with wedged-shaped that compose an arch of stones are called voussoirs. In general they are arranged symmetrically to the keystone or central block.

In the arch made up by building stone, the blocks are wedge-shaped following the arch curvature. However, an arch constructed by bricks (with constant thicknesses) should vary the layer of mortar from the intrados to the extrados to allow the desired curvature.

The block in each abutment on which lays the last voussoir or brick is called skew-back. The surface of the skew-back where the arch starts is called springing and the interior and exterior side of the arch are named intrados and extrados respectively.

The highest point of the arch is known as the crown whereas the lower sections of the arch towards the springing are called haunches.

The rise is the vertical height of arch from springing level to the crown of the intrados and the span length is the distance between the supports of an individual arch along its longitudinal axis. The width is the transverse dimension perpendicular to its span.

The walls that hold back the fill from the extrados till the level of the roadway are known as spandrel walls. The wing walls are the ones at the abutment of a bridge, which extends beyond the bridge to retain the earth behind the abutment. Sometimes tie-bars attached to pattress plates are used to provide restraint to the spandrel walls.

The parapets lie on the spandrel walls and have a protection function against possible collisions of vehicles. Multi-span bridges require piers or intermediate supports between adjoining bridge spans.

Foundations are generally classified into three types: shallow foundation, deep foundation or above rock. Knowing the type and materials with which the foundation is built, as well as their state and the geotechnical properties of the ground is essential for the analysis of the bridge, and can be a major cause of uncertainty.

The fill material is placed in the spandrels between the arch barrel and the road surface and retained laterally by the spandrel walls or wing walls. It normally consists of granular material with low quality as gravel or building debris, which may have been excavated for the foundations or is waste from the construction. Normally, it helps the drainage of the bridge avoiding water accumulation and therefore an increase loading. As a consequence, it is worth to know the current properties of the fill as the degree of compaction, saturation or lateral confinement.

2.2 STRUCTURAL ELEMENTS

In this section the characteristics and typologies of the structural elements are presented. Being these the arch, infill, spandrel walls, abutments, piers and foundations.

Arch

As stated before the arch is the principal structural element in masonry arch bridges. This element works by shape and is made up by materials with almost no traction strength. It has the function to collect the loads from the infill and carry them to the foundations. Therefore, the arch and the infill work together and their behaviour are dependent on the pressure of the abutments.

The arch barrel may be constructed from dressed stone or bricks. When constructed with bricks, the barrel will be formed in several layers or rings which are usually bonded together and are therefore inherently less robust than those with stone voussoirs.

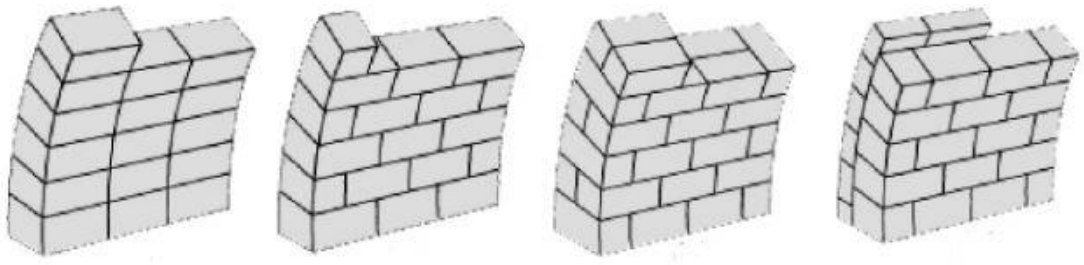

Figure 2-2 types of brickwork most used (Espejo, S. R. 2007).

Arches have a huge variety of types according to their shape and materials. The fundamental geometric parameters are the span length, the rise and the width explained in section 2.1

With regard to their plan view they can be classify as straight, skew and curved bridge. Straight bridges are the most usual due to its simplicity.

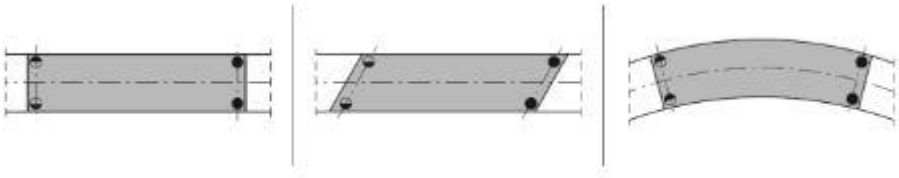

Figure 2-3 plan view of straight, skew and curved bridge respectively, (Hoeckman, W, 2012).

Figure 2-4 shows different types of arch according to its geometric shape.

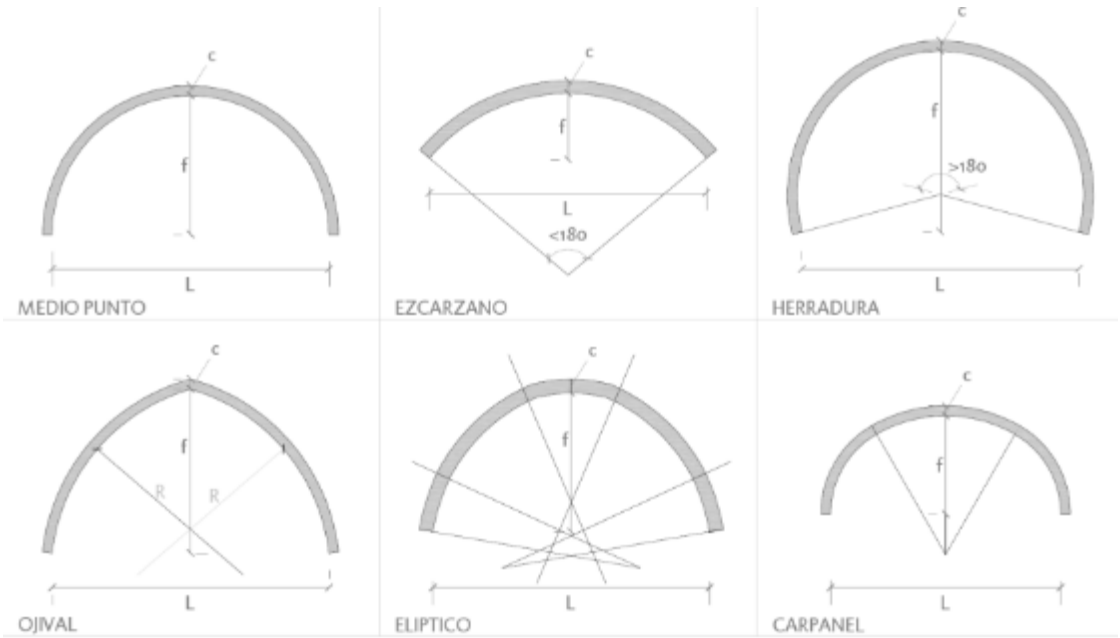

Figure 2-4 different types of arch bridge according to geometric shape (Espejo, S. R. 2007).

Most of the Roman arches follow a semi-circular shape where the rise-span ratio is ½. Segmental arch bridges have a curved arch that is less than a semicircle. An advantage of the

segmental arch is that it allows great amounts of flood water to pass under it, which would prevent the bridge from being swept away during floods and the bridge itself can be more lightweight.

The span length of the bridge has an obvious influence on the magnitudes. Moreover, it affects to the structural performance of the arch. In the bridges with low span, which are the most common, overloads are determinant. However, in large bridges with more than 40 m span length, the dead loads are by far the most important load and therefore they become critical.

It should be noted that the structural shape of the arch often does not match with the one visible from the exterior. This is due to in many cases the haunching or backing in the infill act as a structural part of the arch.

Infill

The infill is any material contained by the spandrel walls and located between the extrados of the arch and the road surface. Therefore, this term includes a huge variety of materials with different characteristics.

Not only is it important to know the type of materials and properties forming the infill, but also its arrangement within the bridge and their degree of compaction, saturation, confinement, etc.

Mainly the infill can be classified in two main groups: one normally composed of stones located towards the springing (haunching); and another composed by loose material placed above the first one.

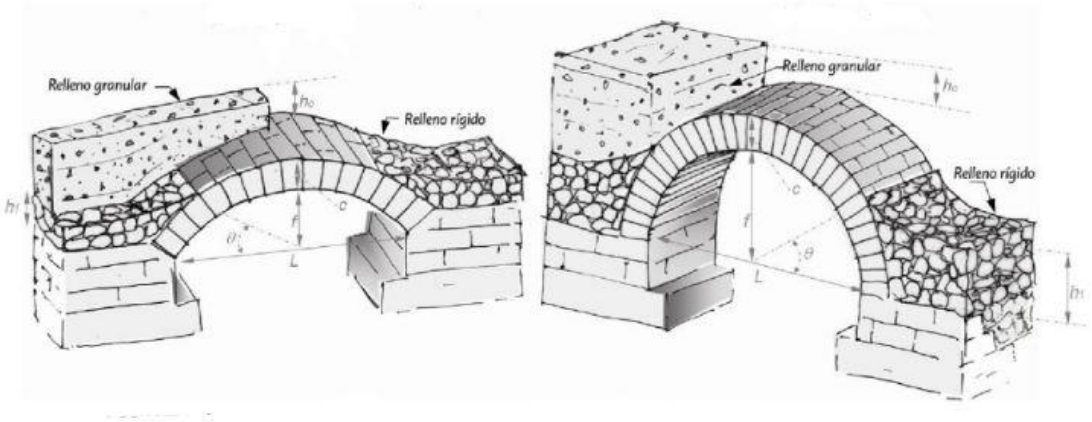

Figure 2-5 infill types representation for a segmental (left) and semi-circular (right) arch bridge (Espejo, S. R. 2007).

The haunching height is a parameter that has a big influence in the ultimate capacity of the structure. The behaviour of the bridge is improved due to the increment of stiffness at the springing.

Un-cohesive sand is often used for the loose material and usually is located near the crown level. Generally it corresponds to natural materials found in the vicinity of the work from the excavation of the foundation. The fill material must be adequately compacted into place to minimize future settlement of the material.

The permanent load of the fill gives an additional load to the arch beneficial for the behaviour of the structure (similar to the presstress effect). In addition, the loose fill is responsible for distributing the additional loads applied on the road surface, and to transmit them to the extrados surface of the arch. The distribution of the loads allows minimizing the local effect of punctual loads.

Spandrel walls

The spandrel walls are the vertical elements which lay on the arches along the bridge. Their principal function is to retain and confine the infill. If the walls do not give lateral confinement to the infill, then any stabilizing pressure of the infill will occur.

Another function of the spandrel walls is that sometimes they give additional stiffness to the structure. Therefore, in the case of solid walls their behaviour can be likened to a big depth beam.

Despite the null tensile strength of masonry, depending on the bonding of the bricks and the linkage with the arch, the whole system can develop a certain flexural strength. However, only under services loads this additional stiffness can appear. When the loads are near the collapse of the structure some cracks appear at the union and then both elements arch and walls have independent behaviours.

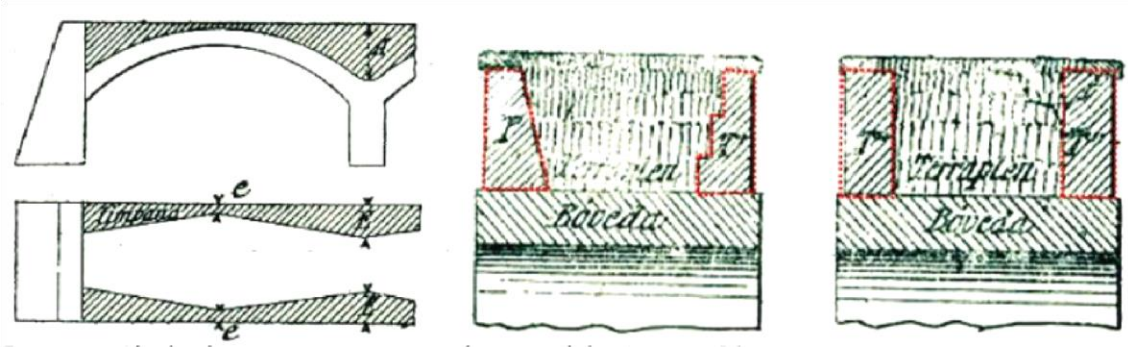

Figure 2-6 typical sections of spandrel walls (Ribera 1925-32).

The exterior surface is flat and vertical whereas the interior one can have a light slope or be stepped increasing the thickness of the walls (Figure 2-6). That geometry follows the law of soil pressures. From the floor view the walls can be straight or have a longitudinal variation having the maximum thickness at the springing of the arch. Again, it seeks to find the best geometry to resist the transversal thrust.

Most of the times the spandrel walls are made with solid bricks. The outer layer is thinner and has better quality and appearance than the inner one.

Abutments and Piers

Abutments are composed by masonry mass supporting the arch barrel and providing resistance to the thrust and vertical loads from the ach.

Piers are intermediate supports between two adjoining arch spans and their main function is to transfer the loads from the arch to the foundations. Also they have to bear all the external loads such as wind or floods.

Sections usually are rectangular and can be classified in two main groups: solid and mixed. Solid piers are made up by a unique type of masonry and mixed piers have two materials. The inner one has a lower longitudinal deformation module than the one used in the exterior faces.

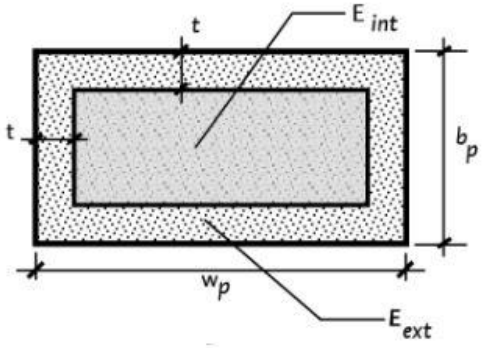

Figure 2-7 typical mixed pier section (Espejo, S. R. 2007).

As it can be seen in Figure 2-8, bended arches have to carry axial loads and bending moments if the loads from both arches are not equal.

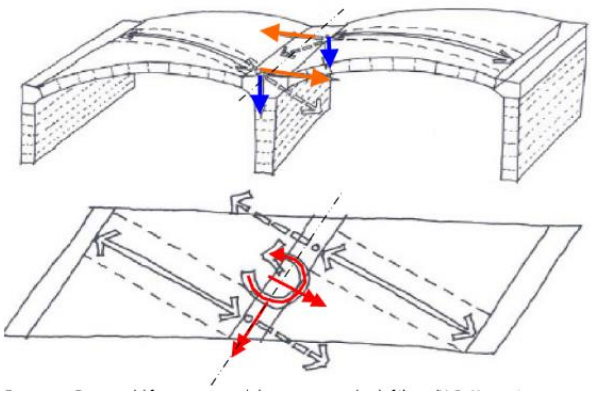

Figure 2-8 pier reactions in skew masonry bridges (Espejo, S. R., 2007).

The main problems in regards to their durability are due to the settlement of the foundations since only few times they reach their ultimate strength.

Moreover, abutments and piers are the elements that receive more impact loads and in the cases where the piers are located at the riverbed with high flow the water can cause damages at their surfaces.

Foundations

Foundations are the part of masonry arch bridges below ground level that transfers and distributes the load from the abutment or piers into the surrounding ground. The failure of this element causes most of the collapses of masonry bridges. Future research should be done in order to understand the interaction between the foundation and ground.

A general classification of foundation is presented as follows:

- Shallow foundations often called by footings are usually embedded about a metre or so into soil. The rock appears at the ground level or is at a lower depth.
- Deep foundations are used to transfer the load of a structure down through the upper weak layer of topsoil to the stronger layer of subsoil below.

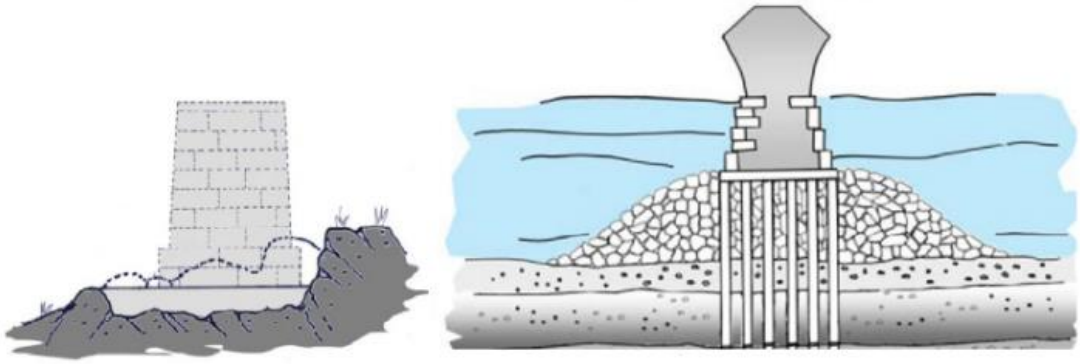

Figure 2-9 shallow (left) and deep (right) foundation (Espejo, S. R., 2007).

2.3 BEHAVIOUR UNDER LOAD OF MASONRY ARCH BRIDGES

The study of curved masonry elements such as arches, domes and vaults should take into account the essentials of the masonry materials. Despite the wide range of possibilities regarding the geometry, assembling and characteristics of different types of masonry, leading to different mechanical behaviour, masonry curved structures have some essential common characteristics (Tralli, A., Alessandri C. and Milani G., 2004):

- Heterogeneity:
  Masonry is obviously a heterogeneous composite material made by clay bricks or stone blocks and mortar. According to experimental evidence, exhibits a non-isotropic behaviour both in the elastic range and at collapse.
- Almost no resistance to tension and good compressive strength
  The tensile strength is quite variable and uncertain; usually the crisis occurs in the interface between mortar and brick.
- High Friction Coefficient
  According to Vasconcelos & Lourenço the friction coefficient for historical masonry is m=0.4 to 0.6. However the normality is lost and the flow rule is not associated.
- Importance of the overall geometry for achieving the equilibrium

In masonry structures where the infill gives a stabilizing effect, the main resistant mechanism is compression. Therefore the geometry of the structure and the position of the loads are determinant in the equilibrium mechanism.

However, at least two additional factors must be taken into account in the analysis of masonry arch bridges. The stabilizing effect is induced by the presence of infill and spandrel walls. And the presence of pre-existing crack patterns which turn into discontinuities in the masonry.

Figure 2-10 depicts the response developed of a masonry arch bridge and how the loads are dispersed from loading point to foundation. The bridge has to bear his self-weight, a uniform live load along its length and a live load applied in the critical zone (between 1/3 and 1/5 of the arch's span).

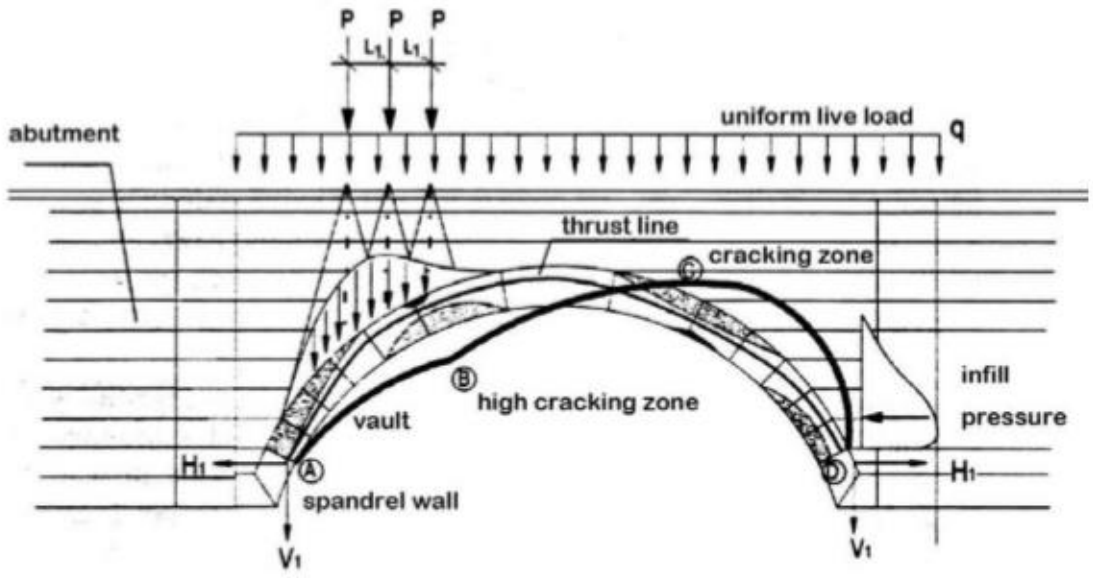

Figure 2-10 arch bridge response to self-weight and live loads (Pereira, R., 2015).

The load of the fill has a stabilizing effect because whose shape approximates the curve of an anti-funicular (this means that only compression is developed on the arch).

However, punctual loads are transmitted from the road surface to the arch through the filling transforming the concentrated load to a spread load on the arch's extrados forming a cone distribution. These actions tend to drive the geometry of the arch and cause the appearance of bending stresses which masonry cannot bear. Due to the low tensile strength of the masonry, usually the arch cannot transfer bending moment to the foundations as shown in Figure 2-10.

The thrust line describes the flow force and thus the arch bridge behaviour. Force is attracted by stiffness. Stiff load paths will always be preferred over more flexible ones, but the more flexible ones will come into play if the stiff ones fail.

Robert Hooke noted that an arch is essentially the mirror image of a hanging chain (un-bonded links). For, understanding, it is best to think of a masonry arch as constructed from un-bounded blocks. Figure 2-11 shows the force flow of an un-bounded block that leads to the formation of the thrust line. Therefore, it's clear that stability depends entirely on the balance of forces and not on the bending strength of the material.

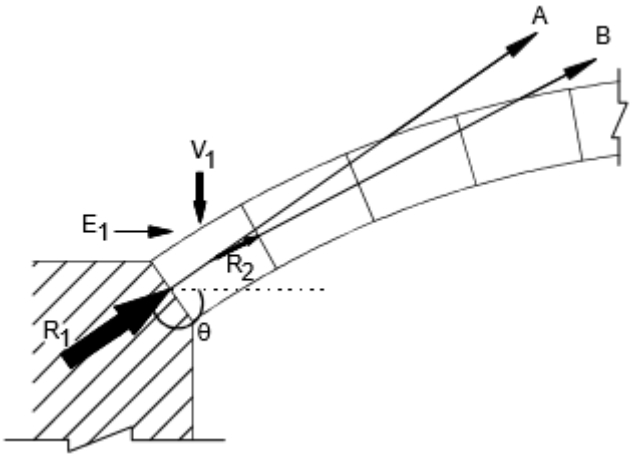

Figure 2-11 flow in an un-bounding block of the arch (Iricen, 2009).

As long as this line of thrust remains within half of arch ring, the arch remains safe. As shown in Figure 2-11, increasing live load will disturb the reactions and result in the arch cracking at points where the thrust deviates greatly from the centre of the arch. This turns to formation of hinges (letters A to D Figure 2-10) leading to the collapse mechanism.

Grey areas in the figure represent the cracked part of the arch where they cannot resist tensile stresses, and black coloured areas show where masonry has reached the compressive strength.

In the case of study where an asymmetric load takes place an arch needs 4 hinges to develop a mechanism and collapse.

Also important is that the soil does not only press vertically downwards, but generate a component of horizontal force too. The spandrel walls bear this transversal lateral thrust which in turn is beneficial to the stability of the arch confining the soil.

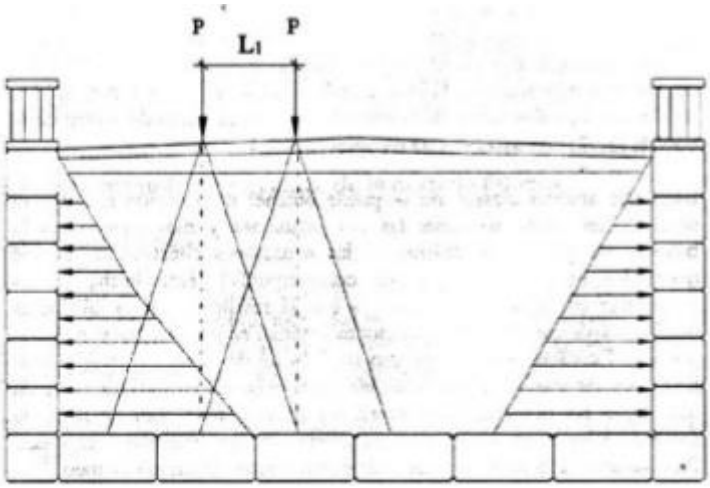

Figure 2-12 bridge cross section and schematic load distribution (Gutierrez, H., 2001).

The increment of this transversal thrust can provoke a failure in the spandrel walls by means of rupture of detachment. In that case, the confinement of the infill will be lost and the road surface damaged.

Once the loads are transferred from the confined infill to the spandrel wall, then they reach the arch and are carried through the foundations. The arch sways taking advantage of the high compression resistance of masonry.

2.4 BRIEF HISTORY OF THE ANALYSIS OF MASONRY ARCHES

Masonry arches are one of the oldest man-made structural systems. But for many centuries they have been built by trial and error methods because their complex behaviour was not fully understood.

This section reviews the history and the development of technology in masonry structures ranging from classical elastic analysis to modern finite element methods.

Seventeenth century

The first recorded investigation into the structural performance of an arch was carried out by Hooke in 1676. This great English engineer realized that the optimal shape of the arch should seek to generate simple compression in the arch. "As hangs the flexible line, so but inverted will stand the rigid arch". Indeed, the behaviour of the arch was simulated as an inverted suspension chain.

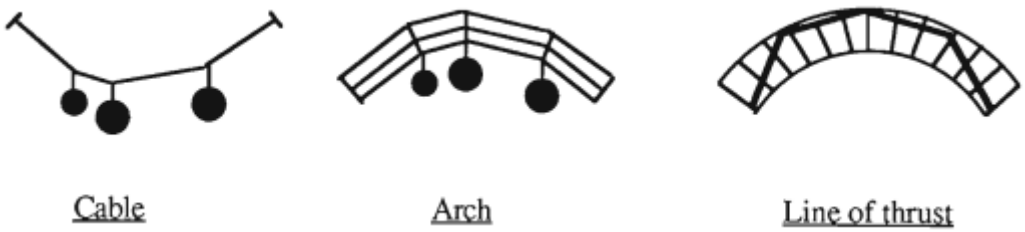

Figure 2-13 line of trhust – Hooke's experimental approach (Yanf Yan, 1991).

Eighteenth century

Since the early eighteenth century French engineers such as Couplet, Frezier or Coulomb, made considerable advancements in the understanding of the structural stability of masonry arches. This was the beginning of a scientific-technical treatment in the analysis of these structures, combining theoretical studies with experimental tests and observations on failure.

Couplet by testing model arches found that arches collapsed by breaking into four pieces by forming a failure mechanism. Afterwards, the studies and observations of Couplet concluded that it is only necessary to find one line of thrust contained within the arch boundaries that satisfies the equilibrium conditions to ensure stability.

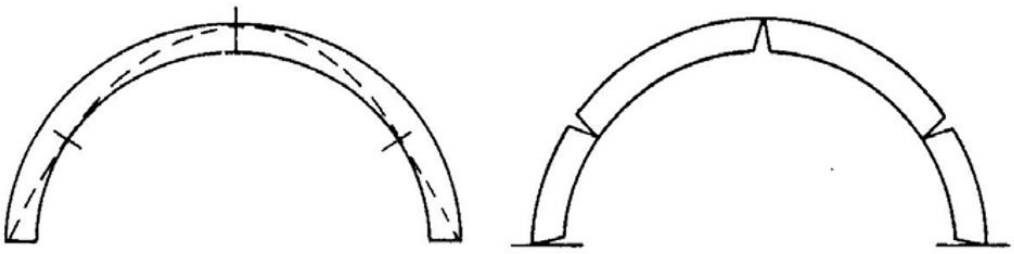

Figure 2-14 failure mechanism breaking the structure in 4 pieces (Huerta, S., 2001).

Nineteenth century

Later on, in the 19th century, engineers as Clapeyron, Navier, Barlow or Castigliano proposed complete analysis methods based on the theory of elasticity. The Italian engineer, Castigliano, incorporates the strain energy method and derived a linear relationship between load and displacement prior cracking. He was the first to calculate the displacements in the structure.

Unfortunately, these methods of analysis may produce large errors because only consider displacements in the arch and assumed that the supporting abutments remain rigid. As a consequence the results should be treated with caution.

From twentieth century until now

Many engineers developed their own methods for calculation the line of thrust in an arch. Pippard used Castigliano's strain energy theorem and modelled the arch as linearly elastic with two pins at the abutments. He thought that the critical load location was at the smallest fill depth, the mid-span.

In 1981 Heyman developed a mechanism analysis procedure utilising the concept of plastic hinge. The analysis assumed that at the point where the line of thrust touches either the intrados or the extrados, a plastic hinge is formed.

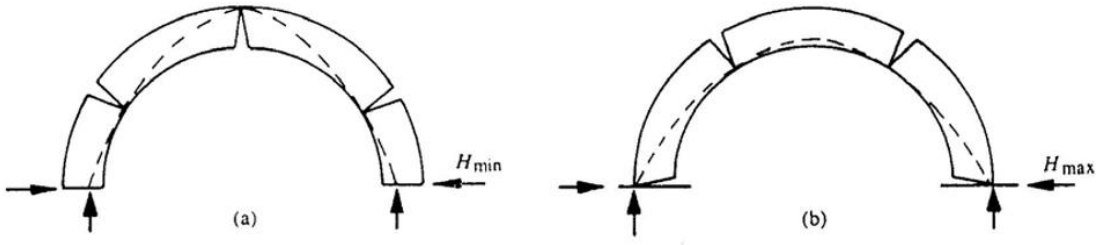

Figure 2-15 semi-circular arch under its own weight: a) minimum thrust and b) maximum thrust (Huerta, S., 2001).

Heyman set the critical load at ¼ of the span length, with plastic hinges under load, crown and abutments. By the following conditions and the limit theorems of plasticity he defined the collapse of the structure (Tralli, A., Alessandri, C. and Milani, G., 2014).

1. The compressive strength of the material is infinite;
2. Sliding between parts is impossible;
3. The tensile strength of masonry is null.

The upper bound (kinematic) theorem If a bending moment diagram is found which satisfies the conditions of equilibrium and mechanism (but not necessarily yield), then the corresponding load factor is either greater than or equal to the true load factor at collapse. This is called the unsafe theorem because for an arbitrarily assumed mechanism the load factor is either exactly right (when the yield criterion is met) or is wrong and is too large, leading a designer to think that the frame can carry more load than is actually possible.

The lower bound (static) theorem If a bending moment diagram is found which satisfies the conditions of equilibrium and yield (but not necessarily that of mechanism), then the corresponding load factor is either less than or equal to the true load factor at collapse. This is a safe theorem because the load factor will be less than (or at best equal to) the collapse load factor once equilibrium and yield criteria are met leading the designer to think that the structure can carry less than or equal to its actual capacity.

The uniqueness theorem If a bending moment distribution can be found which satisfies the three conditions of equilibrium, mechanism, and yield, then the corresponding load factor is the true load factor at collapse. So to have identified the correct load factor (and hence collapse mode) for a structure we need to meet the equilibrium, mechanism and yield.

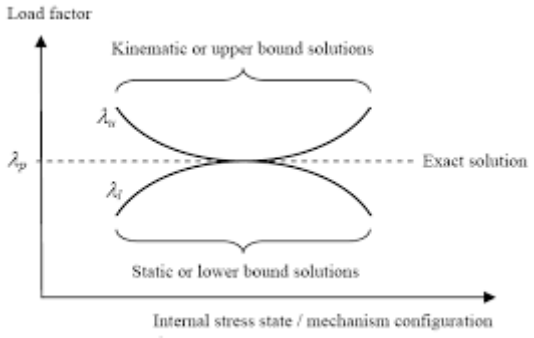

Figure 2-16 upper-bound, lower-bound and uniqueness theorems.

Another method called MEXE was developed in the UK during the World War II based on the work of Pippard. The MEXE method is an elastic analyses theorem, in which the arch is assumed to behave in a linear elastic continuum. Due to its assumptions is one of the most used for the assessment of masonry arch bridges.

At the end of the century, Bridle and Hughes created a computer based energy method of analysing arches for loads up to failure. The arch geometry and stiffness modifies to model the effect of the masonry's inability to sustain tensile stress allowing the formation of hinges. The method provides details of the effective arch section, compressive stresses, shear stresses and deflexions along the arch ring for load increments up to the ultimate limit state.

Finite element analysis became famous in the last few decades mainly due to the development of powerful computers. The advantage of this method over other conventional structural analyses is that it can be used for statically indeterminate structures with irregular shapes and

different boundary conditions. Non-linear material properties can also be defined giving non-linear structural behaviour up to ultimate limit state.

Three dimensional finite element modelling is more realistic but also is more complicated and time consuming.

2.5 MODELLING APPROACHES FOR MASONRY STRUCTURES

As stated earlier, masonry is a material which exhibits distinct directional properties due to the mortar joints which act as planes of weakness. In general, the approach towards its numerical representation of masonry can focus on the micro-modelling of the individual components, units and mortar, or the macro-modelling of masonry as a composite.

- Micro-modelling. This approach of masonry is suited for small structural elements with particular interest in strongly heterogeneous state of stress and strain. Is the best tool to understand the behaviour of masonry allowing all different failure mechanisms. Interface elements are used as potential crack, slip or crushing planes.
- Macro-modelling. This approach is the most used because the interaction between units and mortar is, generally, negligible for the global structural behaviour. Moreover, the computational cost is reduced using this approach. The material is regarded as an anisotropic composite and a relation is established between average masonry strains and average masonry stresses.

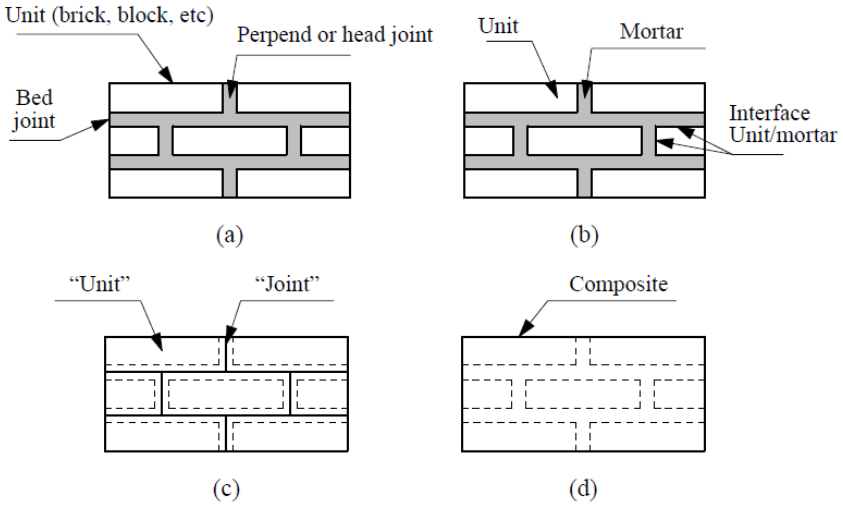

Figure 2-17 modelling strategies for masonry structures: a) masonry sample; b) detailed micro-modelling; c) simplified micro-modelling and d) macro-modelling (Lourenço, B, 1996).

Both approaches of masonry require a thorough experimental description of the material. The use of different testing methods is useful to define the behaviour of masonry which is influenced by a large number of factors such as material properties of units and mortar, arrangement of bed and head joints, anisotropy and dimension of units, joint width, quality of workmanship, degree of curing, environment and age (Lourenço, B, 2013).

3 EXPERIMENTAL TESTING PROCEDURE AND RESULTS

In this part first the geometry and construction phases of the bridge is presented. Moreover, describes how the experiment was carried out and also discusses the final results.

The segmental arch bridge is one of a series of bridges of masonry which was tested in the UPC in a program of experiments led by Professor Pere Roca. This bridge was designed and built during May 28-31 of 2001, and tested on September 12, 2002.

3.1 BRIDGE GEOMETRY

The sizing of the bridge was restricted to the laboratory space and to the tight budget of the program of experiments. Therefore, a small bridge was designed with the following geometry and dimensions:

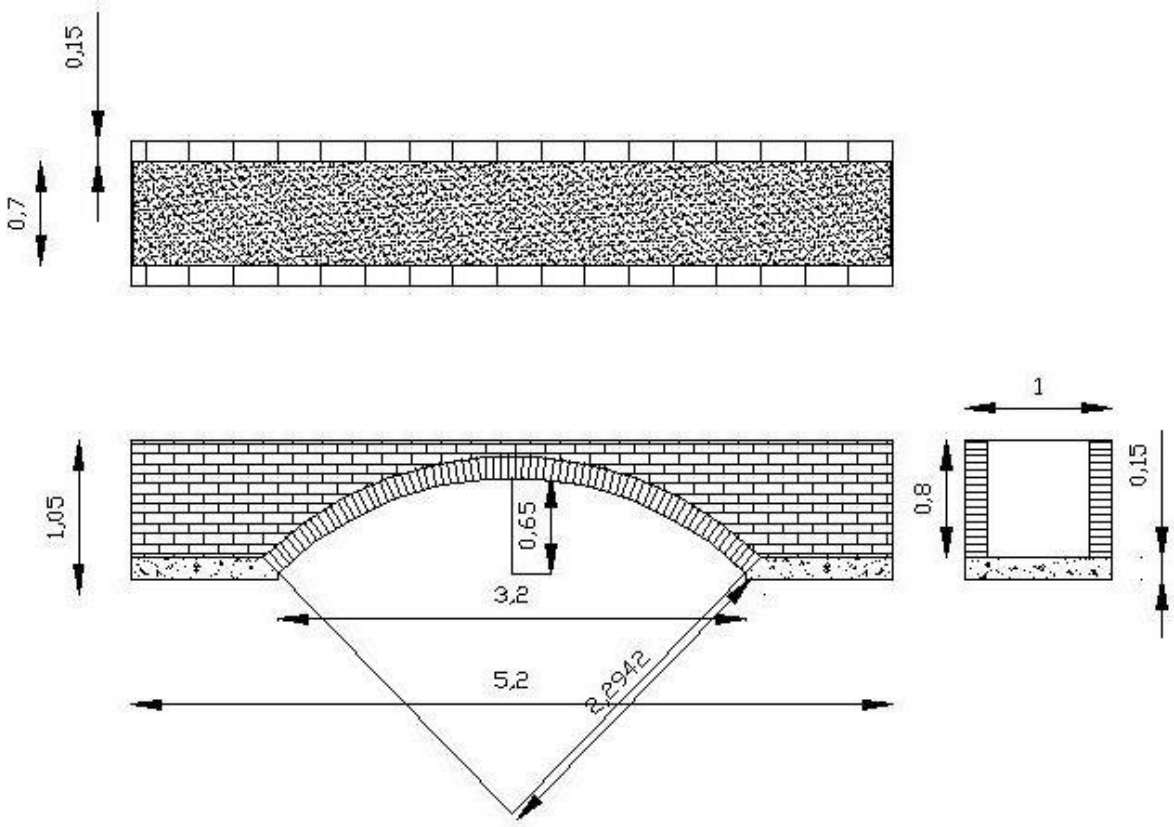

Figure 3-1 geometry and dimensions in meters (Roca, P. and Molins, C., 2004).

As it can be seen in Figure 3-1, the span is 3.2 m and the ring rises up to 0.65 m. The total width is of 1 m. The bridge is built over reinforced concrete footings 1.0 m long and 25 cm thick to transmit the arch's force. Both the arch vault and the spandrel walls are made of brick masonry and have thickness of 14 cm. Sand is used to fill the space between the spandrel walls and the ring.

Steel plates stiffened with steel profiles were installed at the back sides of the abutments to retain the infill and to absorb the horizontal forces. Finally a set of bars with diameter of 25 mm

where anchored to the horizontal profiles stiffening the plates and giving external lateral confinement.

free span (m)	3.20
rise (m)	0.65
total length (with abutments) (m)	5.20
total height (m)	1.05
width (m)	1.00
ring depth (m)	0.14
depth of infill on crown (m)	0.10
maximum depth of un-cohesive infill (m)	0.78
thickness of spandrel walls (m)	0.14
number of steel ties (ϕ=25 mm)	8
loaded point	¼ of span

Table 1 summary of geometrical and construction features.

Approximately the total weight of the masonry bridge turned out to be about 7 tons.

3.2 MATERIAL PROPERTIES

Masonry

The masonry used was composed of solid brick units measuring 13.5 x 28.5 x 4.5 cm and bed joints 1-1.5 cm thick filled with M8 Portland cement mortar. A total of 500 bricks were needed to build the arch ring and the spandrel walls.

Specimens composed of 4 bricks for the compression test (UNE 67-026-94) were prepared immediately after the loading test. The masonry used had a compressive strength of 130 kp/cm^2. Figure 3-2 shows the failure behaviour.

Figure 3-2 compression test of the masnory (Serna, J., 2001).

Infill

The infill was loose sand. Its dry density was 1.55 ton/m^3.

Following the rules NLT-107/91, a Proctor Test was done in order to know the optimum moisture which was approximately of 5% and a maximum density Proctor of 1.86 ton/m3 (Figure 3-3). This last density is the one trying to get through the compaction of infill in the construction process. The friction angle of these sands compacted once took values between 35º and 40º.

Concrete

It was used about 400 litres of concrete for the constructions of foots in order to carry the loads from the arch and the spandrel walls. These slabs were armed with rods B 500 S, with an approximate weight of 40 kg.

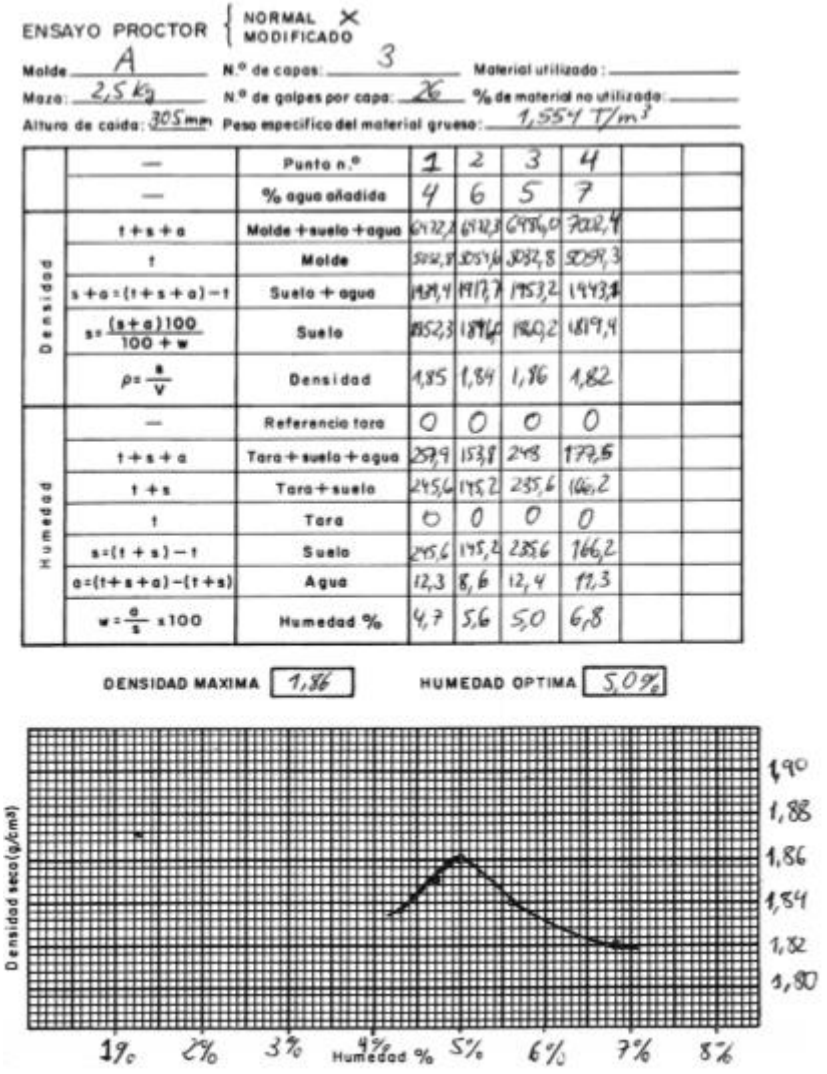

Figure 3-3 proctor test results for the sand (Serna, J., 2001).

Metal profiles and steel bars

As stated before, the abutments were simulated as two metal structures that became rigid by welding steel profiles and were anchored with 8 ties made by steel bars with a diameter of 25 mm. The dimensions of the two steel profiles are as follows:

- 2 rectangular metal sheets of 100 cm^2 and 5 mm. thick.
- 5 vertical profiles with 5 cm square holes inside, 4 mm thick and 100 cm in length welded to each metal sheet.
- 4 horizontal hallow profiles at each side 140x80x6 mm with holes at the end to screw the bars.

Figure 3-4 general overview of the bridge before testing (Serna, J., 2001).

3.3 BRIDGE CONSTRUCTION PROCESS

The bridge was constructed in the technical structural lab of the Polytechnic University of Catalonia.

Concrete slabs

The first step in the construction of the bridge was to build the reinforced concrete slabs on which the arches start. These slabs have a square shape of 1 m and a height of 20 cm. They have an inclined side to ensure the correctness embedding of the arch.

Figure 3-5 formwork and concreting of the slabs (Serna, J., 2001).

Arch and spandrel walls

Once the concrete has hardened and has acquired a minimum strength the formwork of the concrete slabs is retired to proceed with the construction of the arch and the spandrel walls both made by bricks of masonry. For the arch, it was previously built a wooden formwork with the following dimensions and shape:

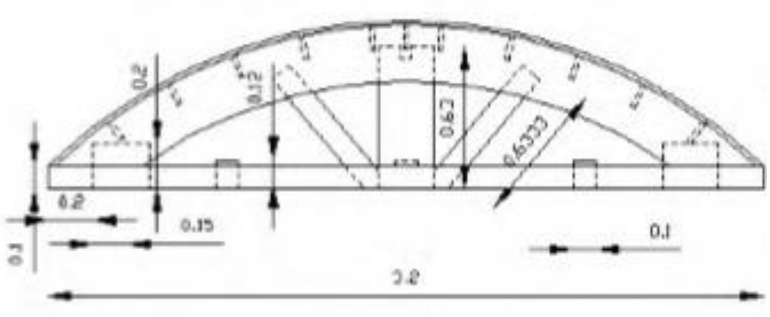

Figure 3-6 wooden formwork for the ring construction (Serna, J., 2001).

The spandrel walls lie on the slabs and ring and they should support the pressure of the infill. It was necessary to wait 28 days for the hardening of the concrete.

Figure 3-7 construction of ring and spandrel walls (Serna, J., 2001).

Steel profiles

Once the construction of all the masonry elements was done the arch could support itself and the weight of the infill, the steel profiles were constructed on each end. The metal structure had two main functions. The first is to contain the soil inside the space during the construction of the bridge. Secondly, the role that restrains the slipping of the slabs in abutment and resist the push force as a result of application of load and movement of the arch.

The assembly of all the profiles was done in the lab by welding. Figure 3-8 shows all the elements used before and after the assembly.


Figure 3-8 method of assembly of the steel profiles (Serna, J., 2001).

Filling and compacting of the infill

Once the steel profiles were placed and all the ties were anchored, the filling process could begin. The filling and compacting process was done in layers of 10 cm in order to control the optimum moisture and reach the maximum Proctor density. The correct amount of water was added to each layer and when the infill was homogeneous they proceed to compact it by vibration.


Figure 3-9 filling and compacting of the infill (Serna, J., 2001).

Densities were verified at various depths at the location where the load will be applied and above the point on the ring symmetrical to the load application. The density results for the 7 layers compacted are provided in Table 2 where layer 1 is the deepest and layer 7 is the most superficial.

Layer	Under load	Symmetrical lcation
1	1.93	1.92
2	1.96	1.98
3	1.98	2.01
4	2.05	1.94
5	1.90	1.98
6	1.98	1.93
7	1.99	2.02

Table 2 average densities of each layer in ton/m^3.

All the measured densities were higher than the value of the maximum Proctor density. This was because the compaction energy of the infill was higher than the one in the Proctor test. The density measurement is of great importance for the numerical methods of analysis because from the density and moisture it can be obtained a good approximation of the elastic modulus E.

Figure 3-10 constructed bridge ready for the loading test (Serna, J., 2001).

3.4 TEST INSTRUMENTATION

The test instrumentation was enough to fulfil the main interests of the experiment which were: to determine the collapse load and to observe and to understand the failure mechanism.

All devices used for the instrumentation, its location and function are described below:

Loading cells

Loading cells were installed on the ties to measure the force on each bar. Only one side of ties were monitored taking advantage of the symmetry of the bridge and load procedure. There was also a load cell below the hydraulic jack to measure the applied load.

Figure 3-11 loading cells at the ties (Serna, J., 2001).

Extensometers

Three extensometers were installed between the ground and the intrados of the ring in order to know the deformation during the loading test. These extensometers were located along the symmetrical axis of the ring under the load, at the centre of the ring and at a point symmetrical to the point of load application.

Figure 3-12 extensometers located under the arch (Serna, J., 2001).

Strain gauges

A total of 4 strain gauges were embedded in the infill to measure the ground motion and to know the horizontal pressure of the infill through the closest abutment to the load, as there would be higher distortion. These strain gauges were placed at different depths and all in the same section as close as possible to the steel profile.

Gauge	Depth (cm)
1	28
2	46
3	58
4	70

Table 3 depth of the embedded strain gauges.

Figure 3-13 strain gauge and compaction device (Serna, J., 2001).

The place where the gauge was embedded was compacted very carefully with a different device to ensure the correctness of the measurements. In Figure 3-13 is depicted the gauge just before being embedded and the compaction device.

Loading system

The loading system was the Hydraulic Jack model ENERPAC RRH-606 shown in Figure 3-14. Below the hydraulic jack a vertical and horizontal steel profiles were used to transfer and spread the load symmetrically. Both profiles were rectangular and with a hollow of 16 cm. Also a spherical joint was attached between them to avoid the transmission of bending moments to the last profile. It is worth to note that no load was directly applied on the spandrel walls.

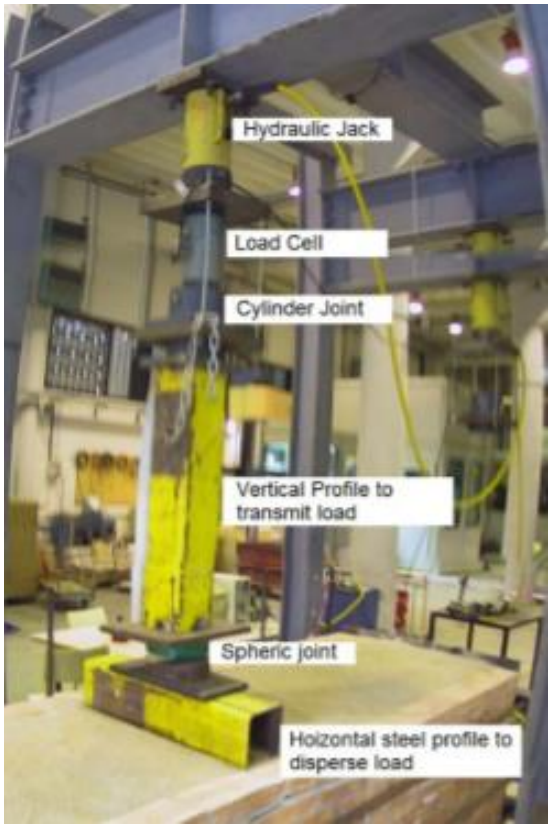

Figure 3-14 loading system (Pereira, R., 2015).

Data acquisition equipment

All of the above mentioned instruments were connected to a data acquisition device which acquires the data from all instruments and displays it on a computer. The only elements that could not be computer-processed in real time were the strain gauges since they were embedded.

Figure 3-15 data acquisition equipment (Serna, J., 2001).

Another device was connected to the hydraulic jack in order to show the load ratio during the test.

3.5 EXPERIMENTAL PROCEDURE AND RESULTS

The loading test was recorded with a video camera and a large number of photos were taken to follow the development of the cracks in the masonry.

As stated before, the load was applied only on the surface of the infill at ¼ of the span. The rate of application of the load was constant over time and equal to 0.05 bar/s, which considering the surface of the loading device is about 1 ton every 4 minutes. This load rate was slow enough to observe the formation of cracks and to label them with markers on the bridge.

As it can be seen in the next figures, the first cracks appear between the spandrel walls and the ring for very low loads. This indicates that a significant elastic deformation of the ring had occurred.

Figure 3-16 cracks before the collapse in the west side (Pereira, R., 2015).

Figure 3-17 general view of the west side and some cracks just before the collapse (Pereira, R., 2015).

Figure 3-18 cracks in the east side for a load below 5 tons (Serna, J., 2001).

Figure 3-19 general view of the east side and some cracks just before the collapse (Serna, J., 2001).

When the load was up to 4 tons a change of slope was recorded in the deformation of the gauges (Figure 3-30) increasing the rate of deformation. Also, since that moment some cracks appeared mostly below the load point and at the point located symmetrically to the load point. That means the formation of the first two plastic hinges were both located in the ring. One of them below the load point and the other at the unloaded side near the top of the ring.

In the same way, when the load increased to 5 tons some cracks started to appear at the springing of the rings which means the formation of two plastic hinges more to produce the collapse mechanism. However, one foot rotated outwards and rose because it had not enough rotational constraints. Later on, when the load was higher both slabs rotated and the movement increased. The shape of these movements is shown in Figure 3-20.

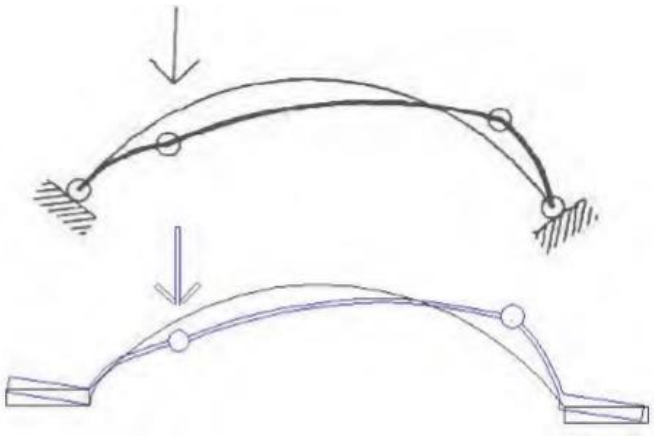

Figure 3-20 mechanism of collapse and rotation of the concrete slabs (Serna, J., 2001).

The rotation movements of the concrete slabs let the ring to rotate at the springing without the formation of plastic hinges. Finally, the mechanism of failure was due to the formation of 4 hinges, two of them due to the load and the other two were implicit before the load because the slabs were not well fixed to the arch.

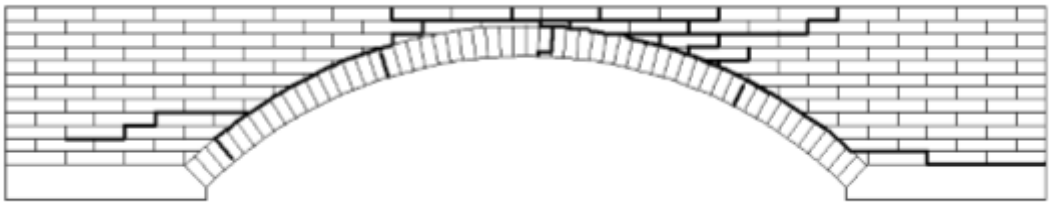

Figure 3-21 distribution of cracks in the arch and spandrel wall (Roca, P. and Molins, C., 2004).

The collapse was reached with an applied load of 5.93 tons. At that point the deformations under the load point suddenly increased turning on large cracks and the rupture was likely immanent. However, before the final rupture could occur, the structure was unloaded.

Figure 3-22 view of the two plastic hinges in the east side (Serna, J., 2001).

Figure 3-23 view of the plastic hinge under the loading point from both sides (Serna, J., 2001).

Figure 3-24 large crack between the ring and the spandrel walls (Serna, J., 2001).

Figure 3-25 risen of the concrete slab and crack at the springing of the ring (Serna, J., 2001).

Figure 3-26 cave-in of the loading system (Serna, J., 2001).

Processing and analysis of results

As stated before, the data acquisition equipment was processed and stored in a spreadsheet. The data measured for all the instruments was recorded every 5 seconds.

Data on the load system

Figure 3-27 shows the applied load by the hydraulic jack over time. As it can be seen, first the bridge was loaded 1 ton because of some limitations of the loading system. Then, the load increased with a constant ratio until the collapse of the structure.

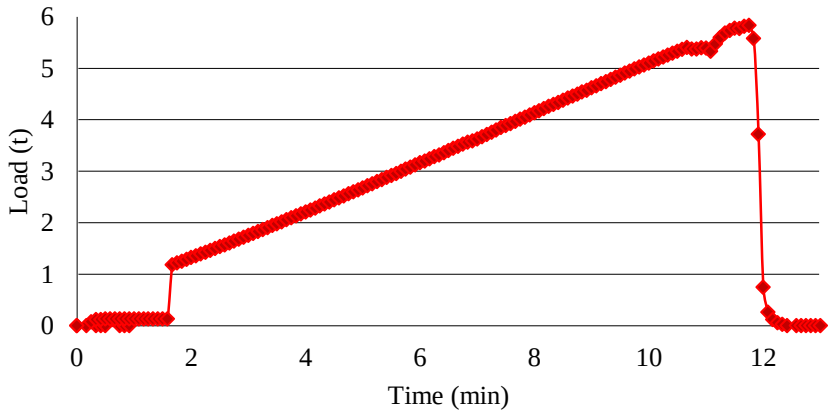

Figure 3-27 evolution of applied load over time.

Data from the gauges embedded in the infill

Knowing the elasticity modulus (10.000 kp/cm^2) and the deformations of the gauges was possible to compute the real passive pressure of the infill.

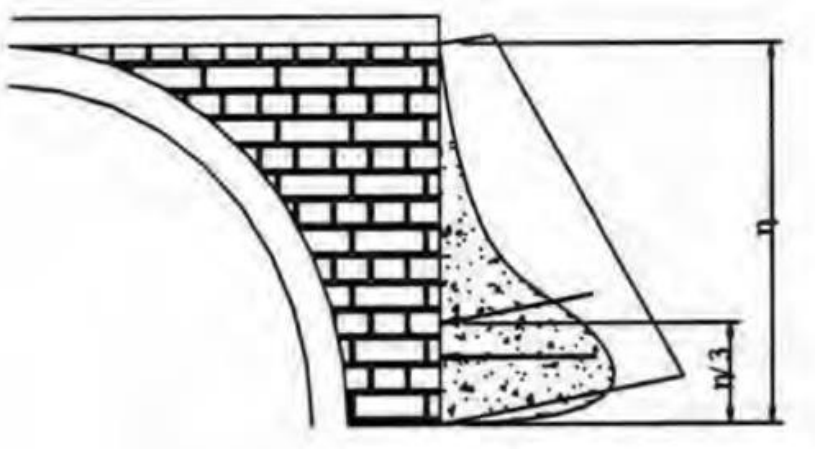

Figure 3-28 theoretical and experimental pressure of the infill (Gutierrez, H., 2001).

Figure 3-29 shows the evolution of the deformation of the infill over time, trying to represent the law of real passive resistance of the infill, in which the thrust force grows to a certain depth and then decreases because of friction experienced by the infill on the upper surface of the concrete slab (Figure 3-28).

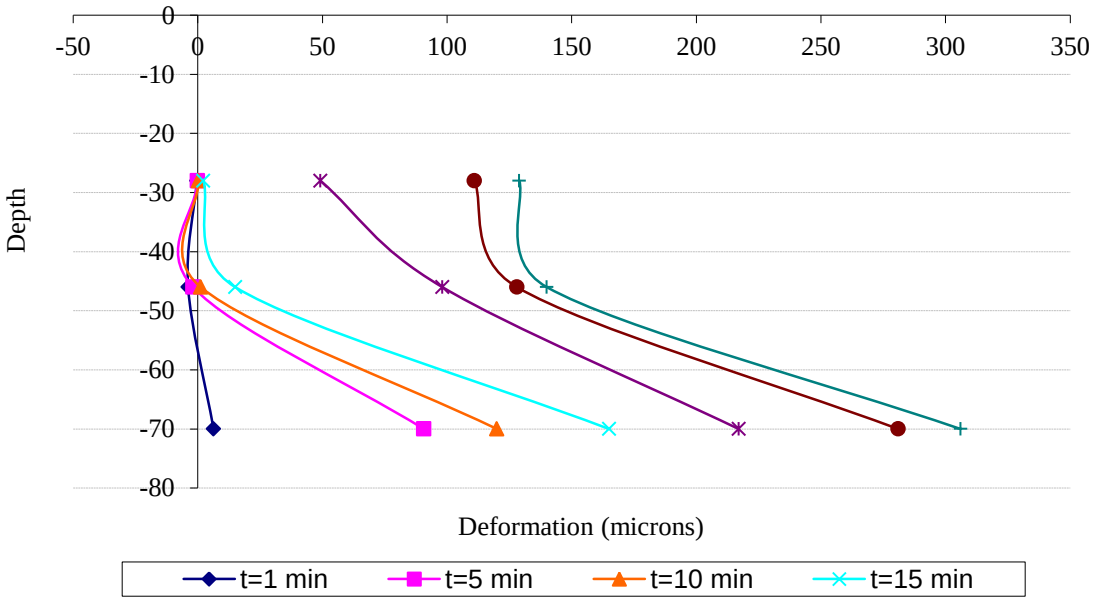

Figure 3-29 gauges embedded evolution deformation in depth over time (Pereira, R., 2015).

In Figure 3-30 it can be seen how the upper part of the infill, from gauge 1 and 2, did not begin to deform until they reach 4 tons of load. As seen in the photos, at this moment appeared some cracks in the ring under the load, the formation of the first hinge and the end of the elastic

behaviour. Gauge 4 started to suffer deformation already in the beginning. Here the deformation was constant until the collapse of the bridge.

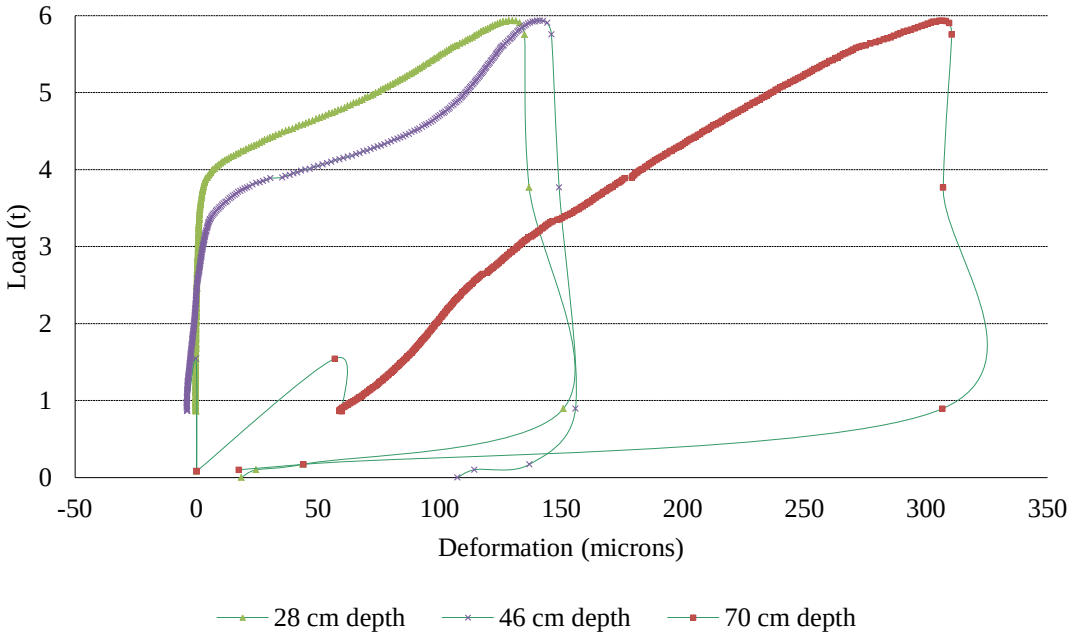

Figure 3-30 load-deformation of strain gauges in the infill.

The data of gauge 3 which is one of the most important to represent the law was not represented due to the incorrectness of the results. Probably the readings of gauge 3 would be higher than those of the lower gauge. The failure of the device made it impossible to check this prediction.

Displacements of the arch

Figure 3-31 shows the data recorded in the extensometers. These devices were located at the half, ¼ and ¾ of the span measuring vertical and small horizontal displacements which are important in the elastic region.

As expected, the point under the loading system decreased whereas the other two points rose. In all points the displacement at the collapse was very similar nearly to 10 mm, or 1/215 of the free span. After the formation of the mechanism, the displacements increased very fast.

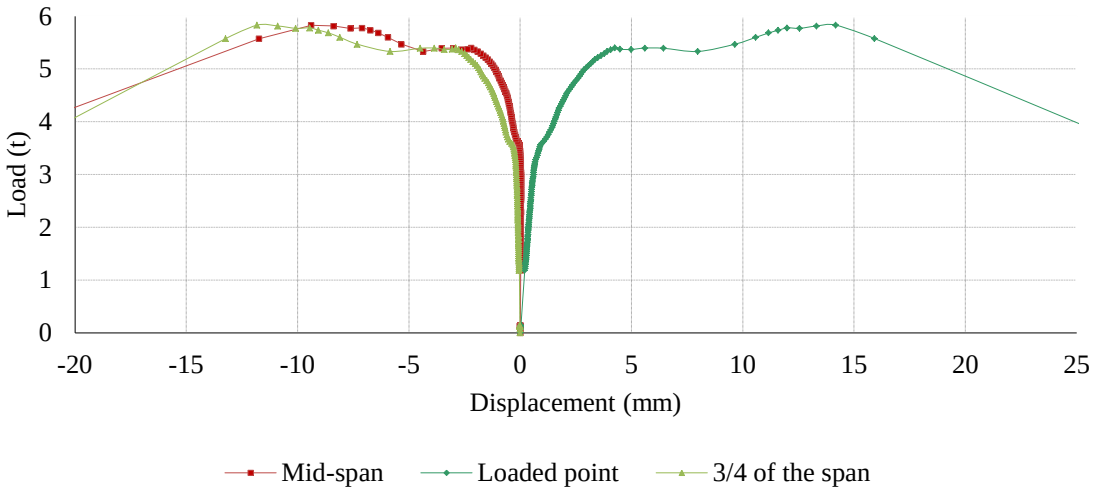

Figure 3-31 extensometers results. Arch displacement at mid-span, loaded point and ¾ of the span.

It can be seen that the slope of the chart is constant until the load reaches 3 tons. Since that moment, some cracks appear and the first hinge is developed.

Axial force in the ties

Figure 3-32 shows the data of the loading cells at the ties. The initial values represent the pre-stress of the ties previous to the test, in order to confine the infill in the abutment.

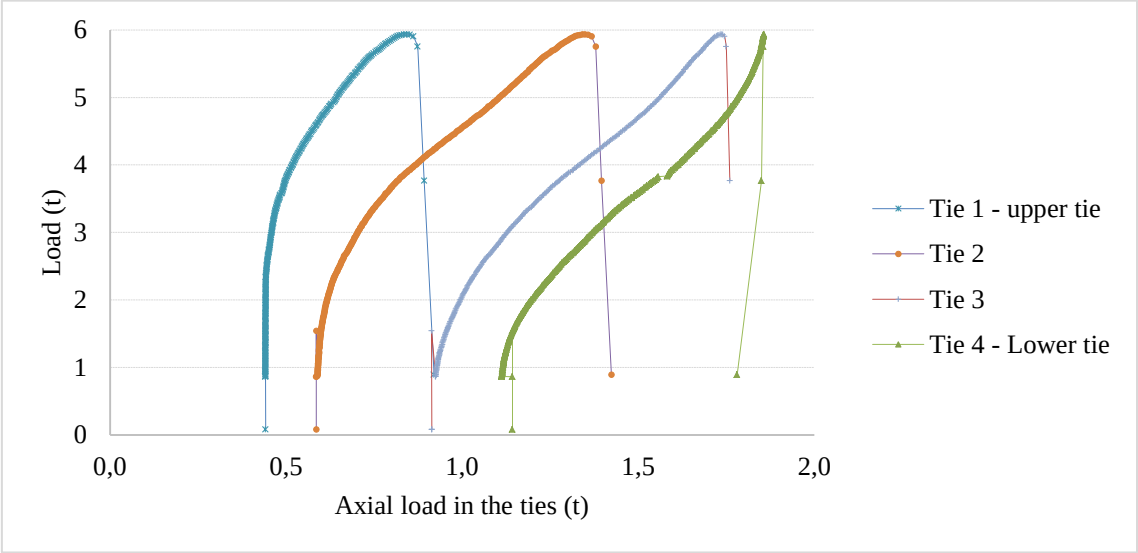

Figure 3-32 evolution of the axial load in the ties.

The behaviour of the axial load was very similar for all ties. The diagram of the upper ties (tie 1 and 2) has two main slopes. First the axial load is almost constant until the applied load is 3 tons. Since that moment some cracks appear and the deformations increased.

In the other hand, lower ties (tie 3 and 4) have an increase of axial load more or less constant from the beginning till the end of the test.

4 PREVIOUS ANALYTICAL AND NUMERICAL PREDICTIONS

This section presents analytical and numerical predictions of the case of study presented in section 3 to predict its general behaviour and the ultimate capacity.

Before performing a complex 3D Finite Element model, it is worth to analyse the key aspects related to the constitutive models and assumptions made in previous works.

4.1 ANALYTICAL PREDICTIONS

Preliminary results, obtained by means of plastic analysis, have provided significant insight on the response of the arch and the role of their different structural components in particular the spandrel walls in the resulting ultimate capacity.

4.1.1 PLASTIC ANALYSIS (STATIC APPROACH)

Roca, P. and Molins, C. in their paper of 'Experiments on Arch Bridges' present preliminary results obtained by means of a simplified method based on the static approach.

Their method considers the contribution to the strength of the cohesive backings and the spandrel walls. The stabilizing effect of the infill weight was also considered. However, because of the relative small volume of the un-cohesive infill, they neglected the lateral confinement of the soil.

The compression strength of masonry is accounted for as a reduction of the available depth of the structural components (in particular, of the thickness of the arch ring). In turn, the maximum shear forces are limited by the Mohr-Coulomb criterion using the values of the cohesion and the angle of friction provided in Table 4.

Component	Property	Average (N/mm^2)	Type of specimen
Brick	Compression strength	56.8	40x40x120 mm prisms
(lengthwise)	Young modulus	12,750	
Brick	Compression strength	51.0	3 stacked 40 mm cubes
(flatwise)	Young modulus	10,450	
Mortar	Compression strength	8.34	Prismatic 40×40×80 mm
	Flexural strength	2.68	Prismatic 40×40×160 mm
	Young modulus	810	
Joint interface	Cohesion	0.36	triplet
	Cohesion	0.33	couplet (biaxial equipment)
	Initial friction angle	45º	"
	Residual friction angle	37.2º	"

Masonry	Compression strength	21.0	4 flat brick prism
Infill (sand)	Specific weight	18 kN/m^3	

Table 4 information on material properties and testing procedure (adaptation from Roca, P. and Molins, C., 2004).

The load is applied on the ring on a surface determined by a 30º distribution across the infill; given the asymmetry of the infill depth, a different distribution is considered at each side of the load axis. The ties have been modelled as a single equivalent one located at an equivalent height.

Table **5** and Figure **4-1** present a set of predictions obtained corresponding to several hypotheses on the contribution of the different structural components of the arch.

Case	Ultimate load / Horizontal thrust (kN)
Experiment	60
Limit analysis	
(1)Arch ring (+ backings in BA2)	15 / 24
(2)Arch ring + spandrel walls	46 / 58
(3)Arch ring + spandrel walls + ties	60 / 74 (17)
(maximum force)	

Table 5 experimental and analytical predictions (adaptation from Roca, P. And Molins, C., 2004).

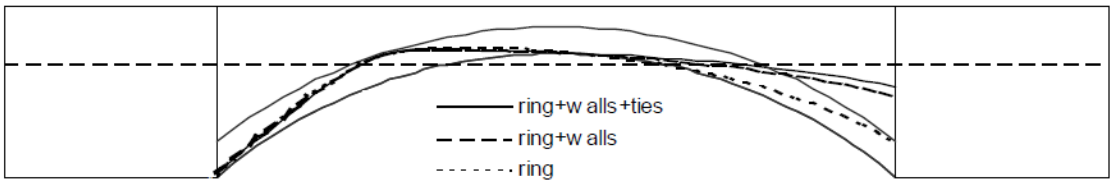

Figure 4-1 plastic analysis (static approach) and thrust lines (1) with the contribution of ring, spandrel walls and ties, (2) without any action from ties and (3) with the arch ring as only resisting element (Roca, P. and Molins, C., 2004).

They concluded that the force that the ties can develop is small because the spandrels are not able to work as a flat arch. Their maximum value is in fact determined by the stability of the abutment closest to the loaded section. The thrust lines have not been allowed to exceed the ring of the arch and invade the spandrel walls except in the lower regions which, according to the experiments, did not develop separating cracks between both elements.

Also, because of the very limited width of the arch, the contribution of the spandrel walls is particularly important. They recommend that any numerical approach aiming at prediction of the ultimate capacity of similar arches should afford an adequate modelling of their strength response. Therefore, a 3D model may be the best to predict general behaviour of both infill and spandrel walls.

4.1.2 LIMIT ANALYSIS USING RING 1.5

Cai, Y. in his dissertation also presents a limit analysis to estimate a lower bound of the ultimate load and the collapse mechanism using the software RING 1.5, see Cai, Y. (2011) for references.

Following the work done by P. Roca and C. Molins, he neglected the lateral confinement of the un-cohesive infill because of its relative small volume, and he only considered the stabilizing effect of the infill weight. The unit weight of the infill and its angle of friction were set to 18kN/m^3 and 38º respectively.

For the sake of simplicity, the structure consists of zero tensile strength joints and the effect of spandrel wall was neglected. The masonry was modelled with compression strength of 14N/mm². Its shear stiffness was limited by a radial friction factor of 6 and a tangential friction of 0.5.

As it can be seen in Figure 4-2, the load is applied on the surface of the infill with a width of 200 mm at ¼ of the ring.

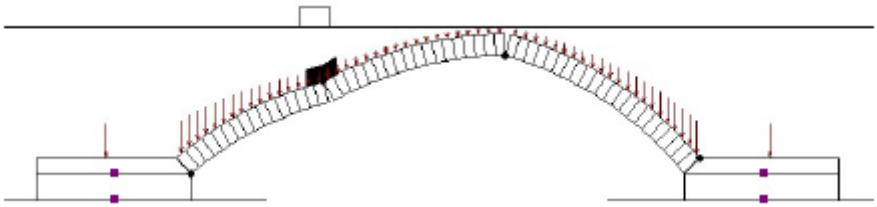

Figure 4-2 collapse mechanism using ring 1.5 (Cai, Y., 2011).

The collapse mechanism was well modelled and the ultimate load was reached at 14.4 kN, very similar to the first prediction made by P. Roca and C. Molins. The fact that the ultimate load is much lower than the experimental one highlights the importance to take into account the spandrel walls and the confinement of the infill.

4.2 NUMERICAL PREDICTIONS

Since the laboratory experiments carried out and presented in section 3, several studies have been done to validate available numerical tools of analysis aimed at the assessment of this type of structures.

The next numerical predictions presented were modelled using the Finite Element Method. Both plane stress and 3D models were developed and analysed with the software TNO Diana which is dedicated to a wide range of civil engineering problems, including structural, and offers a wide range of possibilities in the non-linear field. In the field of Structural Masonry, TNO Diana has already been used in various works and it incorporates constitutive models for masonry.

4.2.1 GONZÁLEZ, J. 2006

Gonzalez, J. (2006) in his dissertation presents two 3D models; one with the software CRIPTA and another using Diana as presented below.

3D CRIPTA model

His first prediction was a 3D model using the program CRIPTA and the postprocessor GID. This model was based on the generalized nonlinear matrix formulation, combined with simple constitutive models suitable to describe the mechanical behaviour of masonry.

This model does not take into account the symmetry of the geometry and load, and consists only of 14 different sections made of 28 rectangular shapes which define the geometry and materials as shown in Figure 4-3 and in Figure 4-4.

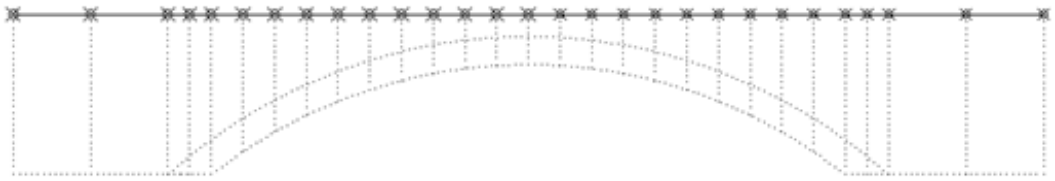

Figure 4-3 3D Cripta model location of sections (González, J. 2006).

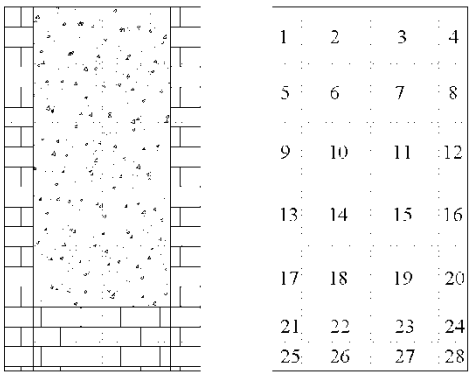

Figure 4-4 3D Cripta model typical section (González, J. 2006).

The results are not presented because of the lack of correctness. Indeed, it was not possible to see the plastic hinges because the arch does not reach the ultimate tensile strength. In this model the bridge works as a compact solid. The displacements and ultimate load differ far from experimental measures.

DIANA 3D model

This time, he modelled half of the bridge taking into advantage geometrical and load symmetries.

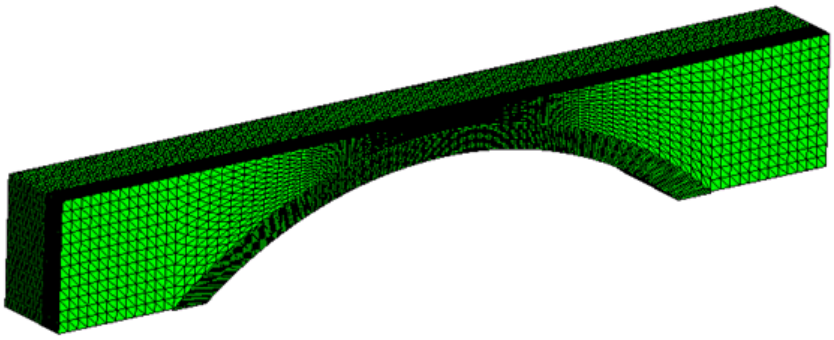

Figure 4-5 mesh of the Diana 3D model (González, J. 2006).

To model the materials two types of elements were used: TE 12L for all the elements of the bridge and the linear element L6 BEN for the ties.

Also, the interface between the arch and the spandrel walls was modelled using the surface interface element T 18IF.

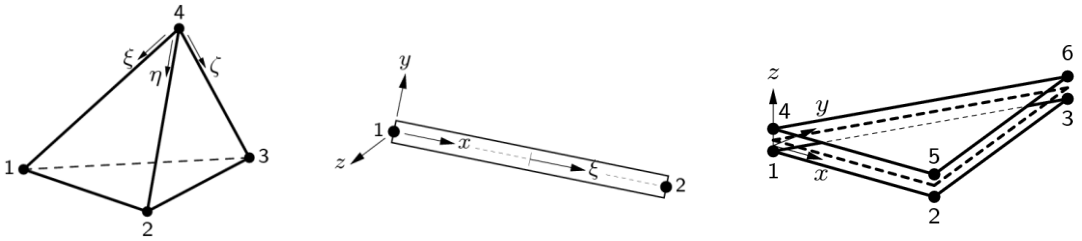

TE 12L L6 BEN T18 IF

Figure 4-6 elements used in the Diana 3D model (Gonzalez, J., 2006).

The masonry followed a macro-model with isotropy properties and a smeared cracking model with a tensile strength of 0.1 MPa, compression strength of 14 MPa, Poisson's ratio of 0.2 and density of 1800 kg/m^3. The Young modulus for the arch (8500 MPa) and for the spandrel walls (10450 MPa) had different values.

The infill had a density of 1800 kg/m^3 and a Poisson's ratio of 0.2. The tensile strength was set to 0.0405 MPa but the numerical model is not specified in the dissertation.

First the self-weight is considered and then a distributed load of 95 kN is applied on the infill surface as in the laboratory test. Load steps were performed with increments of 20% of the collapse load until the convergence of the results.

However, the results did not end up with the same ultimate capacity of the experimental test. As it can be seen in Figure **4-7**, the displacements of the model were very low whereas the bear capacity of the structure was much higher, approximately 42%.

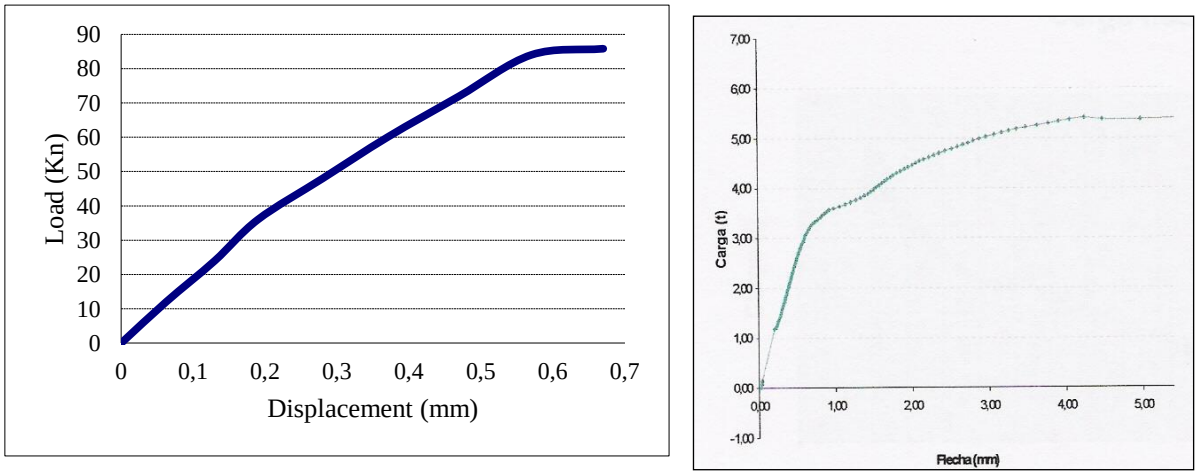

Figure 4-7 load-displacement diagram under the loaded point. Left Diana model and right experimental test (González, J. 2006).

The stresses on the road surface and on the arch were very high because the soil did not spread the load through its volume. However, the general behaviour of the structure was correct. The collapse of the structure was reach after the formation of 4 plastic hinges as shows Figure **4-8**.

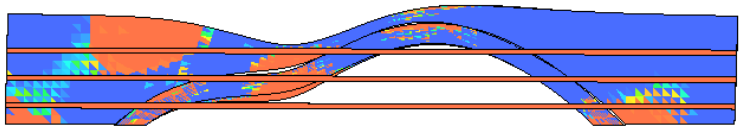

Figure 4-8 deformation and principal stresses (red for tension) of the arch bridge (González, J., 2006).

4.2.2 CAI, Y. 2011 AND FOREST, B. 2012

Previous works (Cai, Y., 2011 and Forest, B., 2012) consist of a finite element analysis using the software TNO Diana to simulate the same experiment.

As the first step, linear and nonlinear analyses were made of several plane stress approaches. The 2D models neglected the effect of spandrel walls since they only consider the effect of the infill above the arch. One year after, in 2012, Forest, B. continued the research of Cai, Y. and made the verification of his models and create a new one.

Both previous works are presented together since all different models present the same modelling approach and overall geometry, in which each component of the bridge was modelled according to its materials and adopted element types.

Plane stress models

Table 6 gives a resume of the plane stress models tested, with different layers of infill, with and without ties and different boundary constraints. In all models the loads considered were self-weight and a pressure load over a concrete block of 20x20cm in terms of load control.

	Constrains	Ties	Infill layers
Model A (Cai and Forrest)	Base and abutments	No	1
Model B (Cai and Forrest)	Base	Yes	3
Model C (Forrest)	Base	Yes	5

Table 6 resume of previous models features.

Figure 4-9, Figure 4-10 and Figure 4-11 show the materials and constraints of the models presented in Table 6.

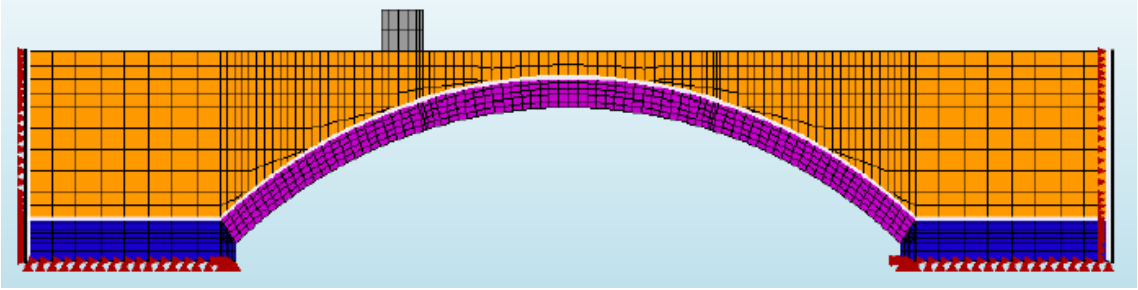

Figure 4-9 plane stress model with one layer of infill, no ties, fixed abutments and base (Pereira, R., 2015).

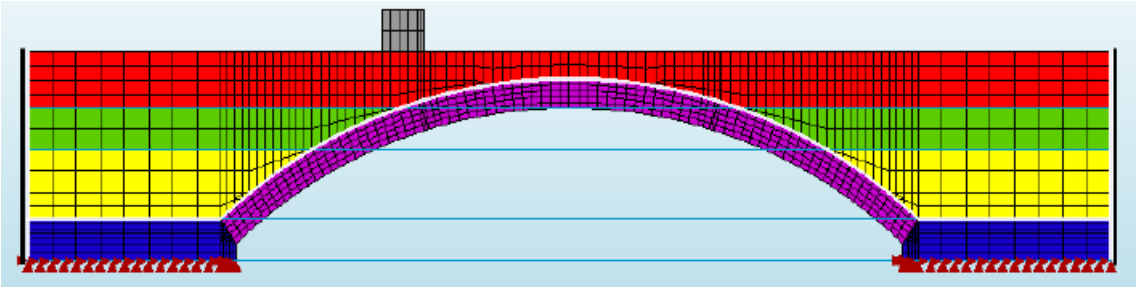

Figure 4-10 plane stress model with three layers of infill, with ties and base constrained (Pereira, R., 2015).

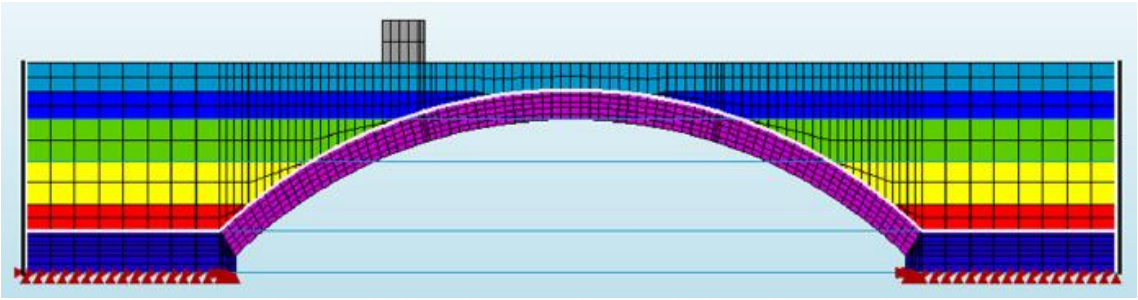

Figure 4-11 plane stress model with five layers of infill, with ties and base constrained (Pereira, R., 2015).

Elements

They made a very accurate model which consists in different element types according to the geometry of the model, materials, desired structural behaviours, accuracy of results and numerical convergence method.

Figure **4-12** depicts all the elements used: plane stress, beam, truss, interface and spring elements.

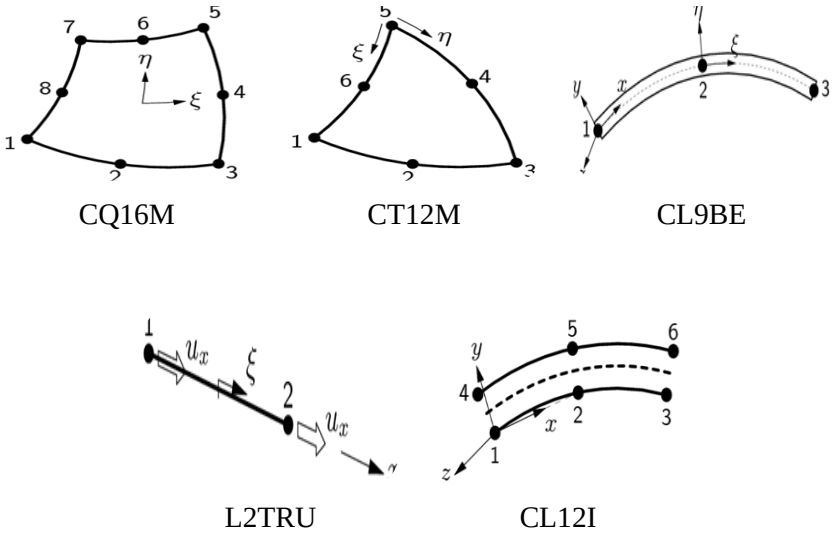

Figure 4-12 elements used in the plane stress models Cai, Y. & Forrest, B (Diana-User's Manual 2016).

- Plane stress elements: eight-node quadrilateral CQ16M and six-node triangular CT 12M, isoparametric plane stress elements were used for the infill, arch and abutments. They are both based on quadratic interpolation, what is recommended when performing non-linear analysis in plane stress models and each node has two degrees of freedom.
- Beam elements: three-node, two-dimensional beam element CL9BE model the steel plates of the abutments. Each node has 3 degrees of freedom, translations in x and y and rotation around z. The strains vary linearly along the central line of the beam.
- Truss elements: two-node directly integrated (1-point) truss element L2TRU were used for the ties. These elements only work in tension and fulfil the condition that the dimensions perpendicular to its axis is small in relation to its length.
- Interface elements: CL12I interface elements based on quadratic interpolation were used to model the boundary between the infill and the other components of the model and also the joint between arch ring and spandrel wall.

Material models

This section describes the constitutive models and strategies adopted to model the material properties. The models incorporate the physical non-linearity of the material for the infill, masonry and interfaces. However, steel and concrete were modelled as linear elastic materials.

- *Masonry*
  As stated before, in the two-dimensional models the spandrel walls were neglected. The arch ring was modelled as a continuum following a macro-model.
    - Multi-directional fixed crack model:

  This non-orthogonal crack model is one of the available in Diana and uses the concept of smeared cracking with strain decomposition into an elastic strain and crack strain, $\epsilon = \epsilon^{e} + \epsilon^{cr}$.
  The sub-decomposition of the crack strain gives the possibility of modelling a number of cracks that simultaneously occur. In order for successive crack initiation to occur, two criterions must be satisfied simultaneously: The principle tensile stress exceeds the maximum tensile stress; and the angle between the principle tensile stress and the existing crack exceed the threshold angle. There exists a local crack strain vector for each `fixed´ crack existing in the element and by appending them an assembled crack strain vector is formed.

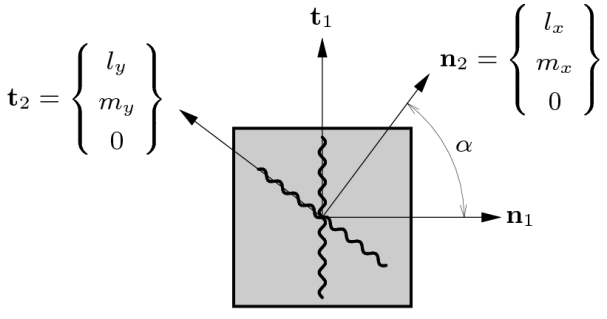

Figure 4-13 multi-directional fixed crack model (Diana User's Manual, 2016).

- Tension softening

Masonry was developed using linear softening function based on fracture energy.

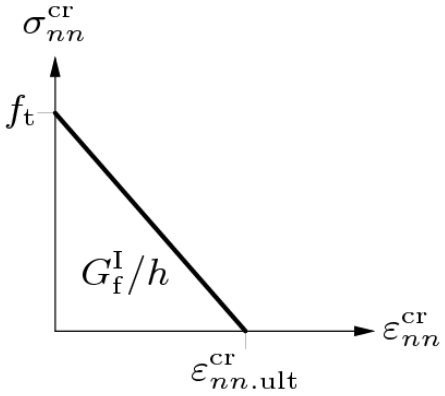

Figure 4-14 tension softening function (Diana User's Manual, 2016).

- Compression behaviour

To model the nonlinear behaviour of the masonry between the stress and the strain they chose a parabolic predefined function as follows.

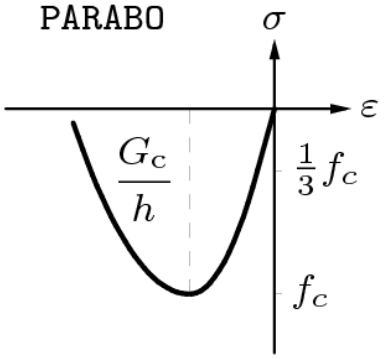

Figure 4-15 parabolic compression function for total strain crack models (Diana User's Manual, 2016).

- Shear behaviour

After cracking occur the shear stiffness is reduced linearly until ultimate shear strain is reached. Thus constant shear retention was used.

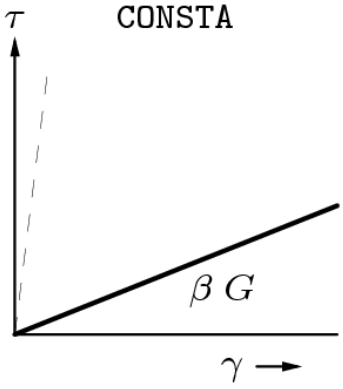

Figure 4-16 constant shear retention for total strain crack models (Diana User's Manual, 2016).

- *Infill*

  In the first model the infill was modelled as a uniform material with constant elastic modulus. Then, they study the effect of increasing the elastic modulus with the depth and they made a model with three and five horizontal layers. The elastic modulus was calculated in function of the depth according to the equation $E = 0.32 \cdot z$, where z is the depth in cm and E is given in N/mm^2.

  - Mohr-Coulomb plasticity model: The yield condition of Mohr-Coulomb was used in all models assuming associated plasticity. The parameters needed were the cohesion and the frictional and dilatancy angles that had the same value.

- *Steel and Concrete*

  For the sake of simplicity, both steel and concrete were modelled as elastic isotropic materials because in any case yielding occurs. Therefore, the only material properties needed were: Young Modulus, Poisson ratio and saturated mass density.

- *Interfaces*

  The Coulomb friction criterion was the interface constitutive model used for the interface elements. The non-linear parameters adopted for the soil were cohesion, friction angle, and dilatancy angle, the last adopted equal to the friction angle assuming associated plasticity.

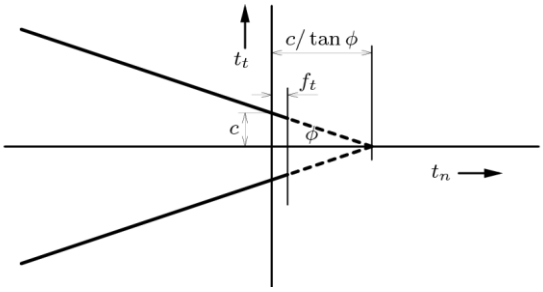

Figure 4-17 coulomb friction criterion (Diana User's Manual, 2016).

3D models

Cai Y. made a first 3D model with ties, fixed footings constraints and 3 infill layers. Afterwards, B. Forrest tried to verify the previous model and since he did not succeed he made a new one increasing the infill layer up to 5.

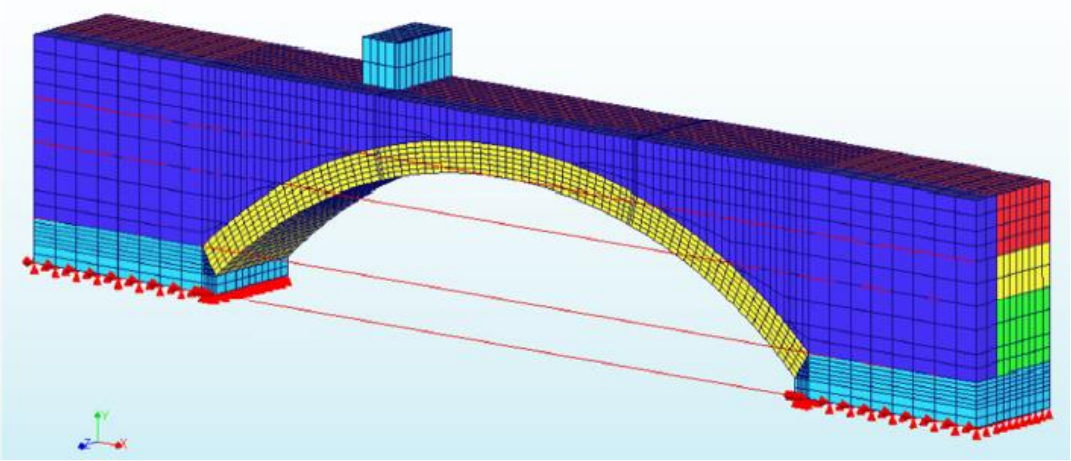

Figure 4-18 3d model with 3 layers of infill, with ties and base constrained from Cai, Y. (Pereira, R. 2015).

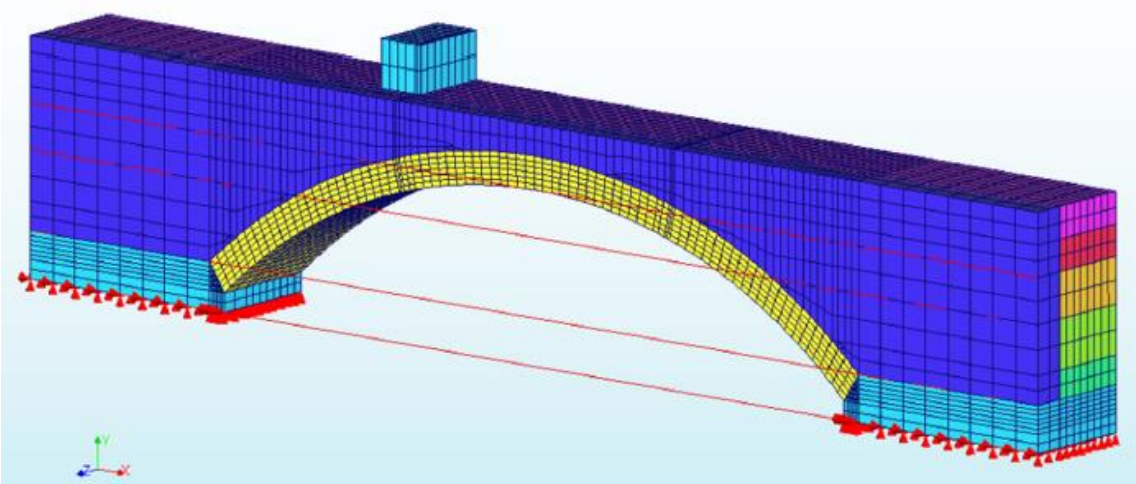

Figure 4-19 3d model with 5 layers of infill, with ties and base constrained from Forrest B. (Pereira, R., 2015).

Elements

Figure 4-20 depicts the elements used in the 3D model.

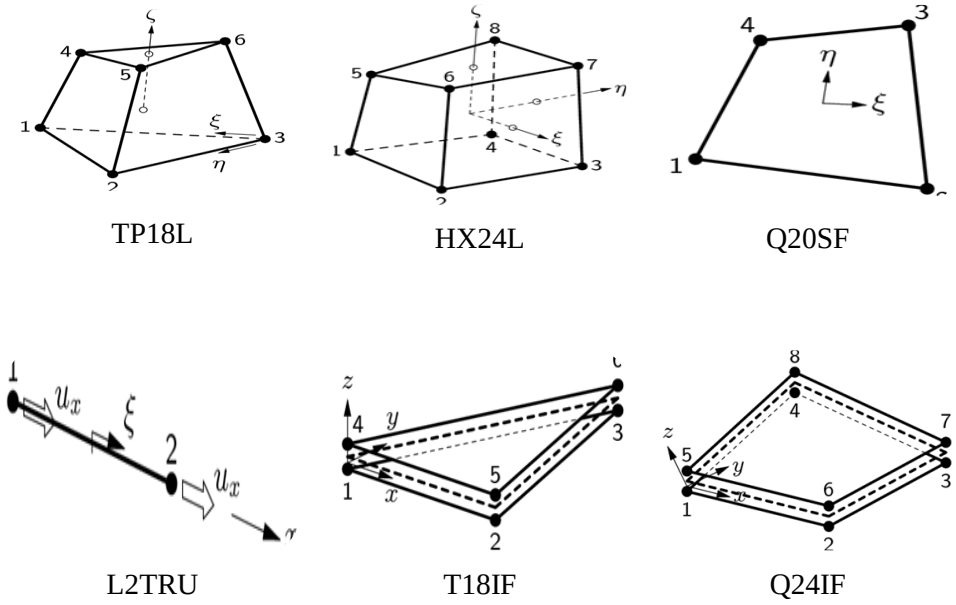

Figure 4-20 elements used in 3d models (Diana User's Manual, 2016).

- Regular elements: six-node TP18L and eight-node HX24L isoparametric solid elements were used for the infill, arch, spandrel wall and abutments. The basic variables are the translations u_x, u_y and u_z yielding a constant strain and stress distribution over the element volume.

- Shell elements: four-node quadrilateral isoparametric flat shell elements were used to model the steel profiles. The basic variables of regular flat shell elements are the translations u and the rotations φ yielding a constant strain and stress distribution over the element.

- Truss elements: as in the 2D model, two-node directly integrated (1-point) truss element L2TRU were used for the ties. These elements only work in tension and fulfil the condition that the dimensions perpendicular to its axis is small in relation to its length.

- Interface elements: T18IF and Q24IF interface elements between two planes were used.

Strategies adopted

The constitutive models of the materials were the same as in the plane stress models.

However, the 3D models adopted the following strategies:

- The longitudinal symmetry was used in order to reduce the computational cost. Therefore, only half of the thickness of the bridge was modelled applying the appropriate constraints at the symmetry plane.
- The load was applied only on the soil road surface over a concrete block of 20x20 cm section, and 36 cm long.
- These models incorporate the spandrel wall with the same material as the ring. Also friction interface elements were introduced between the spandrel walls and soil infill.

Results and conclusions

The results were similar for all plane stress models and provide a good overall understanding of the structure and collapse mechanism. Indeed, the deformation was as expected since the area under loading point descended whereas the part symmetric to it rose and it was possible to see the formation of four hinges in the arch ring.

However, the non-linear analysis stopped before peak, and the maximum load and displacement under the arch were far below the experimental data. For example, in model C presented above, the maximum load and displacement was around 16 kN and 2.77 mm respectively, while in the experiment the peak values were around 60 kN and 12 mm.

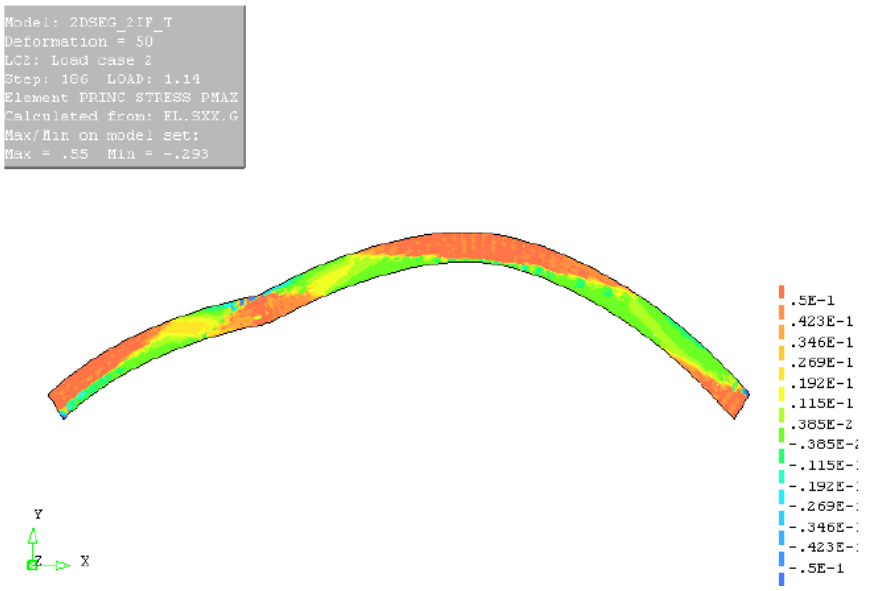

Figure 4-21 principal stresses on the ring for the non-linear analysis of model c (Forrest, B., 2012).

Figure 4-22 from the dissertation of Cai, Y., shows the stress evolution in the arch ring. Even if the stress values may not be enough for a hinge formation, the order in which the stress concentrations appear had the same order than in the experiment test. As it can be seen, the first hinge starts at the left springing, followed by the region under the load, middle span and right springing.

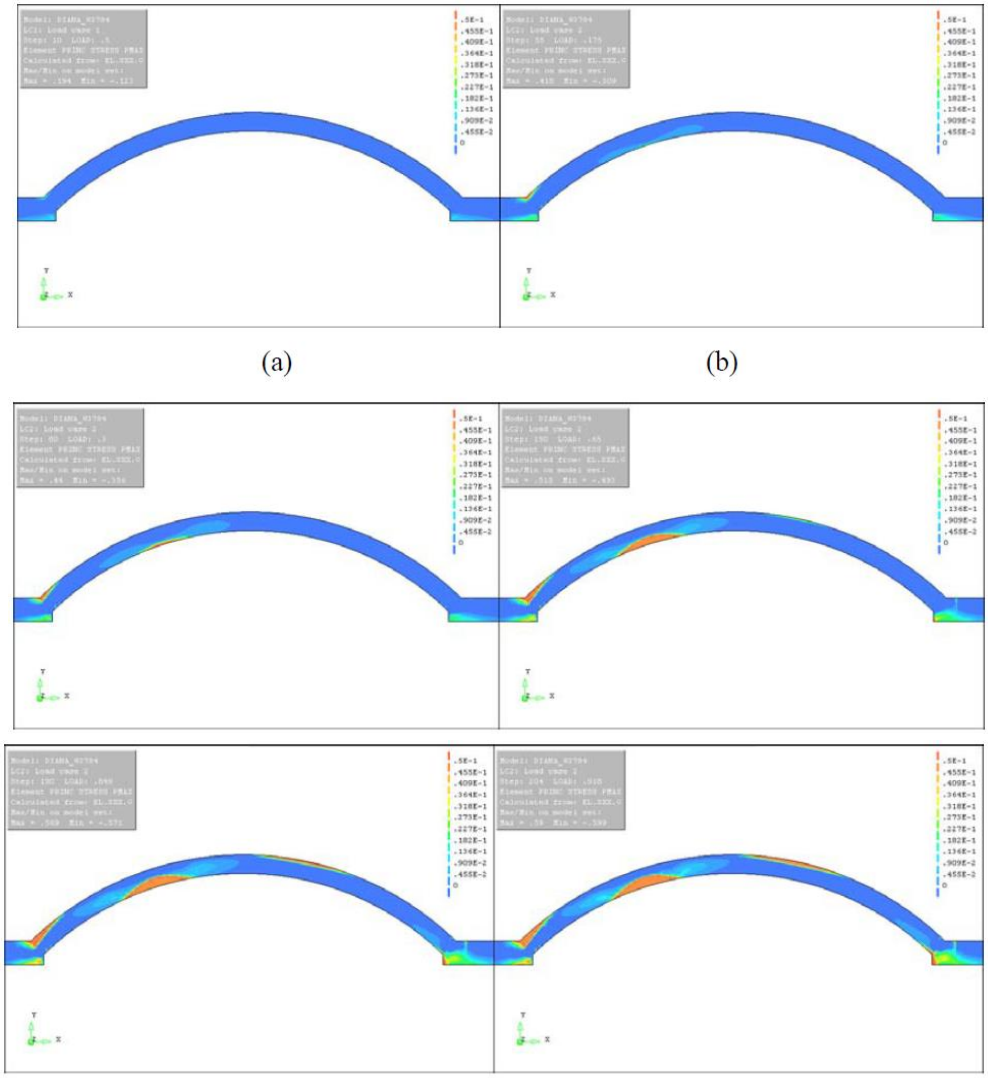

Figure 4-22 stress evolution loading process in masonry arch (a) 0kn, (b) 2.45kn, (c) 4.2kn, (d) 9.1kn, (e) 11.9kn and (f) 12.9kn (Cai, Y., 2011).

Cai, Y. studied the influence of the tensile strength in masonry regarding the behaviour of the model. Figure **4-23** shows the load displacement diagram acquired from a node on intrados of arch under the loading point.

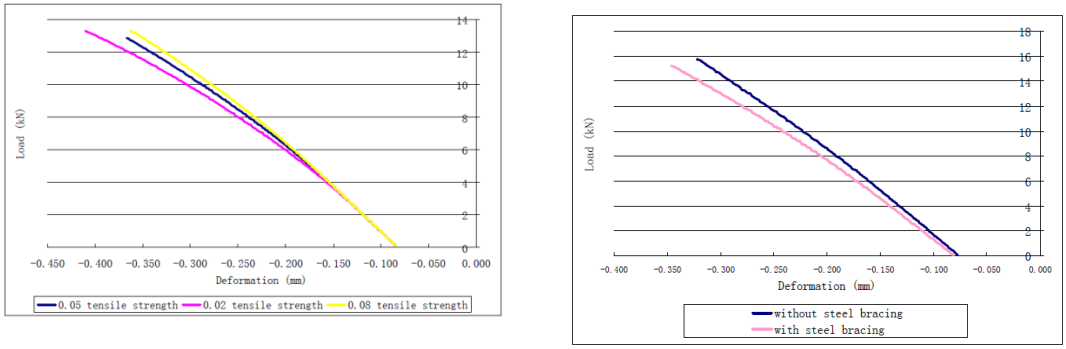

Figure 4-23 load displacement diagram for different tensile strength of the masonry (left) and for model with horizontal constrains in the abutment and a model with ties and without lateral constrains (right).

It can be observed that decreasing masonry tensile strength makes the structure less stiff and able to undertake more displacement. Also, when the horizontal constraints in the abutments are removed and the model incorporates steel ties, the arch ring results in a more flexible model.

Forrest B. perform a verification of the models of Cai Y. and he end up in more consistent models especially in terms of interface elements orientation, that proved to be important in yielding good result. The models of Forrest B. had better convergence and allow to reach higher loads but without any indication of post peak behaviour in the load displacement diagram. For the same load the verification models yielded into the same result in terms of stress and displacement.

The 3D model of Cai Y. was also verified. He got values closer in magnitude but the overall shape of the deformed mesh and the contour plots did not appear to match the results presented in Cai's dissertation. The only difference in Forrest's model was that he reduced the initial stiffness of the interfaces from 1000GPa to 5 MPa. The change was made for the reason of reducing the tensile stress in the extrados of the ring. When stiff interface elements were used, the difference between the stiffness of the ring and interface was large, resulting in increased tensile stress on the elements in contact with the interface.

The results presented in both dissertations had similar results but not exact. Thus, the linear analysis in the 3D model could not be verified. The nonlinear analysis also proved to be unsuccessful since did not lead to stable solution.

4.2.3 PEREIRA, R., 2015

One more time, the dissertation of Pereira, R. in 2015 was aimed at assessing the capability of different approaches on reproducing the real structural response of the same brick masonry arch bridge.

In his work only plane stress models with nonlinear homogenous materials and discontinuities modelled with interface elements were analysed using the software TNO Diana 9.6. Moreover, a large sensitivity analysis of the models to the variation of particular parameters was performed.

Elements

Pereira, R. took advantage of previous models and used mostly the same elements presented before. However, in order to allow the lifting observed in the buttresses he attached one-node translation spring/dashpot SP1TR elements to the nodes at the base of the concrete slabs.

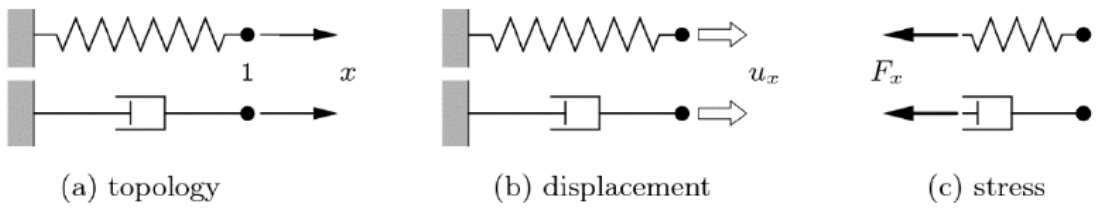

Figure 4-24 SP1TR element (Diana User's Manual, 2016).

Load implementation

To overcome the difficulty in obtaining post-peak results in the non-linear analysis there was the need of implementing a displacement control of the load, avoiding non-convergence when, after the peak, the stiffness is rapidly reduced. This was done by changing the applied load of the previous model to an applied displacement.

He took the model C made by Forrest B. and only by changing the load control to a displacement control the analysis went considerable further due to better convergence of the model (Figure 4-25, right).

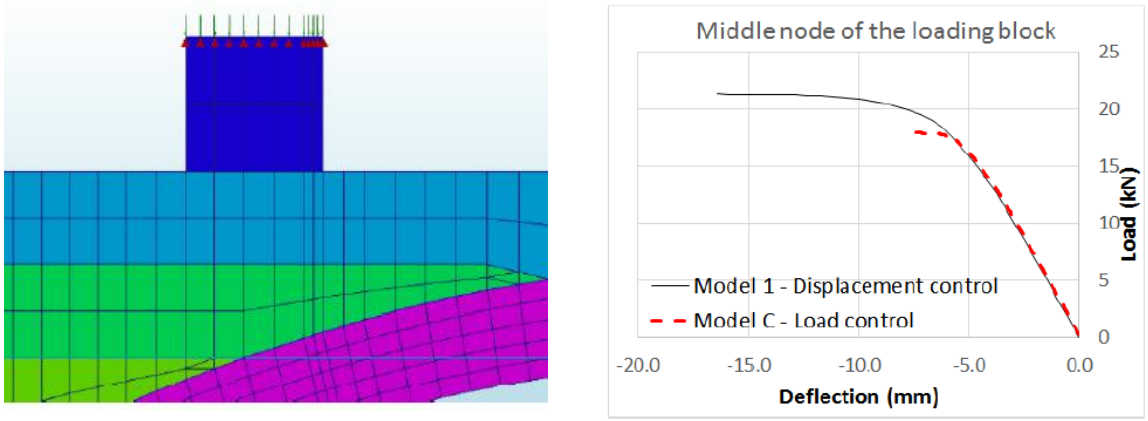

Figure 4-25 new supports attached to allow displacement control (left) and load vs displacement results at the point of application of the load (right) (Pereira, R., 2015).

In Diana software displacement control has to be applied at supported nodes, thus vertical supports were set to the upper nodes of the loading block as depicts Figure 4-25 (left).

It was necessary to make the analysis in two phases since the new supports constrain the vertical displacements in the upper nodes of the block, relieving the effect of the self-weigh on the ring. Therefore, in a first stage only self-weight was considered and the supports where the displacements are applied did not exist in the model. And in a second stage, the supports were implemented and the live load was applied using displacement control on the concrete block.

Results and conclusions

As stated before, Pereira, R. made a very large sensitive analysis. He realised that the material properties of the infill have a big influence in the ultimate capacity. Indeed, Figure 4-26 shows the dramatic effect of the cohesion in the capacity of the arch. Also, in the right plot of Figure **4-26** it can be seen that the numerical and experimental load displacement present a very similar overall behaviour. In both cases, there is a change of slope in the beginning of the loading and a second just before the ultimate load, indicating a similar collapse mechanism.

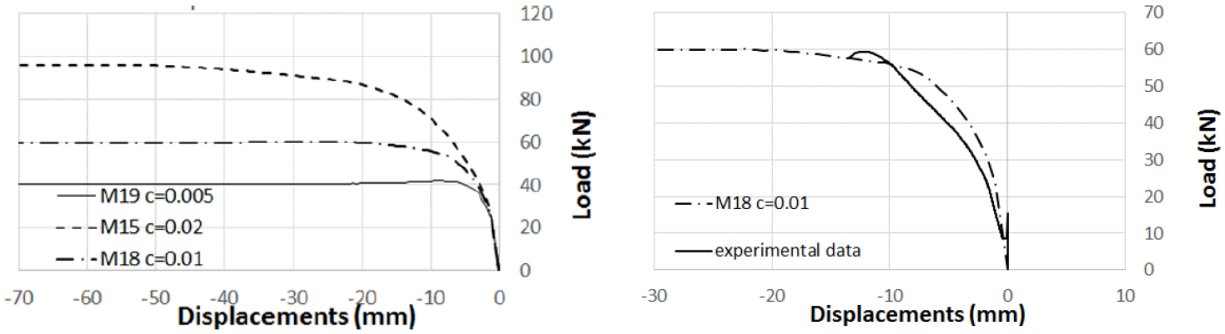

Figure 4-26 load vs vertical displacement at l/4 for different soil cohesion values (left) and both the experimental data and the best fitting result obtained (right) (Pereira, R. 2015).

He used the same constitutive models of the materials than Cai Y. and Forrest B. The Mohr-Coulomb model used for the infill was very simple, without hardening in compression or tension cut-off and provided inaccurate results. He decided to model the area under the load as masonry to allow the continuation of the analysis. Despite this configuration is not the most realistic as it affects the distribution of the load over the extrados of the arch, it provided satisfactory results regarding the deformed shape and ultimate load.

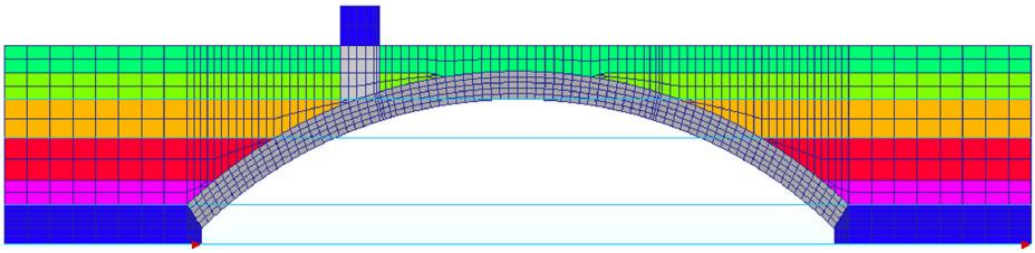

Figure 4-27 plane stress model mesh where the colours show the materials used: grey for the masonry, blue for the concrete and the other colours for the 5 soil layers (Pereira, R., 2015).

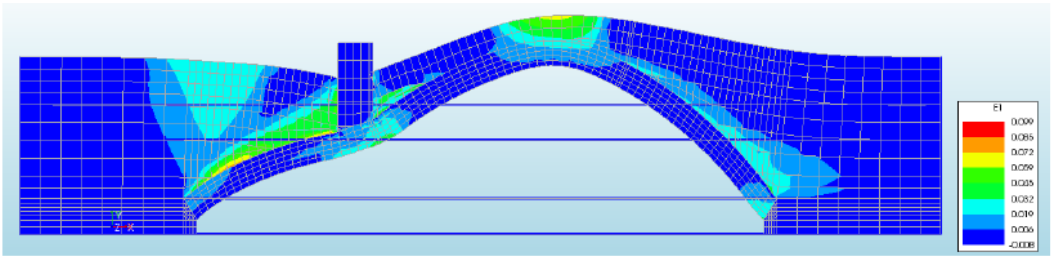

Figure 4-28 total strains in the bridge at 20mm vertical displacement (Pereira, R., 2015).

Also, he performed some models with and without ties and with different support conditions at the base. As it can be appreciated in Figure **4-29**, in the model with fixed base the higher change of slope happens at a load slightly higher than in the models less restrained. Also, the ties represent plays a remarkable influence in the ultimate load.

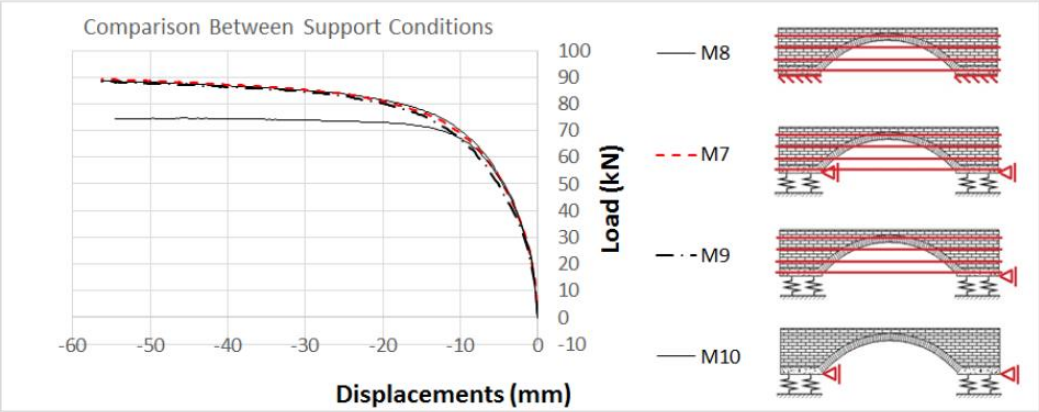

Figure 4-29 comparison between different support conditions (Pereira, R., 2015).

To conclude, Pereira R. made a very good work to understand deeply the behaviour of plane stress models and overcome convergence problems. By implementing displacement control was possible to obtain post-peak results.

The modelling of the soil was not enough good because the model adopted has not hardening and thus, it was needed to model the area under the load as masonry to allow the continuation of the analysis.

After his work, it was proven that plane stress models can predict well the collapse mechanism, but to produce a model that follows the complete load displacement diagram of the experiment other constitutive models need to be implemented. Moreover, in this particular case, where the spandrel walls account for almost 30% of the overall width, both the infill and the spandrel walls are very important in the structural response and it is highlighted the use of 3D models.

5 DEVELOPMENT OF NEW 3D MODEL

Before the 3D model, previous bidimensional models were set up in order to get familiar with the software Diana and with the non-linear analysis. These 2D models helped to get preliminary results testing material properties and boundary conditions with a low computational cost.

It is well kwon that the best way to represent the structural behaviour of an arch bridge is by using accurate 3D models. Indeed, as stated before, bidimensional models cannot show both infill and spandrel walls and their interaction.

The bidimensional models made by Pereira R. were provided and were very useful to understand how to implement the non-linear analysis with two phases and also how to export output files to excel. Also, a 3D model provided by the Professor Climent Molins was analysed in this dissertation and the geometrical data of the mesh was adopted because it contains all the geometric features with interfaces. However, this model was not able to run a non-linear analysis and the material properties and boundary conditions were changed.

All these previous models were made with older versions of Diana. Therefore, the first step was to update the files so they could be correctly read it by the last version. The 3D model was provided in txt files (.dat) with all geometrical data of the mesh, properties of the materials, support conditions and applied loads. A problem of working with .dat files is that the geometry cannot be edited in the geometry editor of the software but need to be changed manually in the text if it is needed.

All the models were fixed and analysed using the software Diana 10. Several constitutive models and material properties were tested for both plane stress and 3D models. However, in this section only the modelling and results of the 3D models are presented.

5.1 ELEMENT TYPOLOGIES

The adopted element types were chosen according to its geometry and desired structural behaviour. For the 3D model the elements used are described below:

Solid elements

Both HX24L and TP18L solid elements are used to model the abutments, infill, arch ring, spandrel wall and load block. The HX24L element is an eight-node isoparametic solid brick element whereas the TP18L is a six-node isoparametric solid wedge element.

The TP18L yield a constant strain and stress distribution over the element volume. However, in the rectangular brick element the strains and stress σ_{xx} and ε_{xx}, σ_{yy} and ε_{yy}, σ_{zz} and ε_{zz} are constant in x, y and z direction respectively and vary linearly in the other directions.

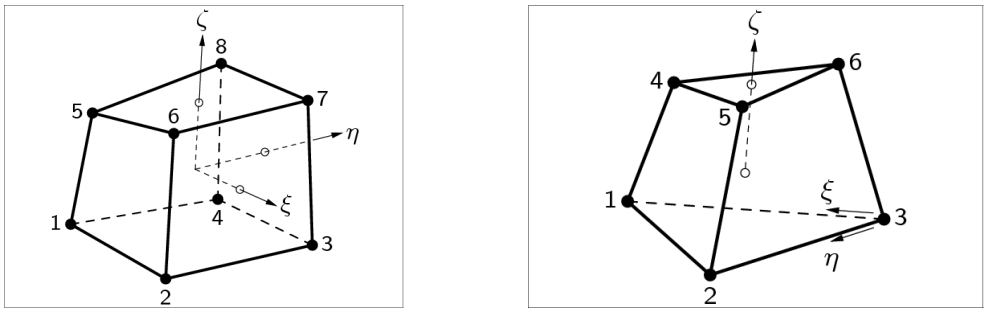

Figure 5-1 brick 8 nodes HX24L and wedge 6 nodes TP18L elements (Diana User's Manual, 2016).

Flat shell elements

Four-node quadrilateral isoparametric flat shell elements Q20SF are used to model the steel plates. The plate bending is according to the Mindlin-Reissner theory. The geometry and the displacements are interpolated by bi-linear functions.

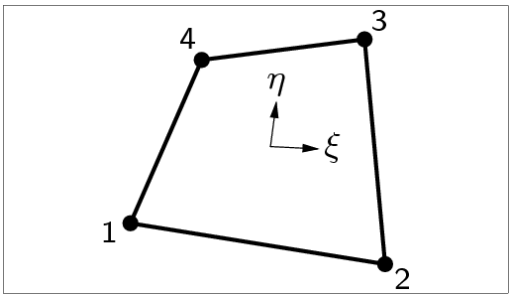

Figure 5-2 quadrilateral 4 nodes Q20SF element (Diana User's Manual, 2016).

Truss elements

Two-node directly integrated truss elements are used to model the ties. The polynomial interpolation for the displacement yields a strain ε_{xx} which is constant along the bar axis.

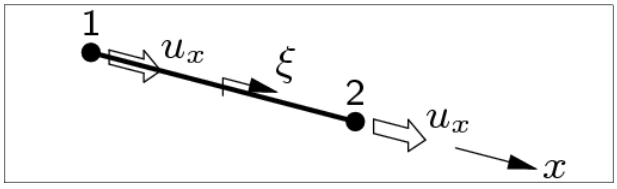

Figure 5-3 straight, 2 nodes L2TRU element (Diana User's Manual. 2016).

Interface elements

In order to simulate the sliding and cracking between different structural element, plane triangle 3+3 nodes T18IF and plane quadrilateral 4+4 nodes are used. Both elements are based in linear interpolation.

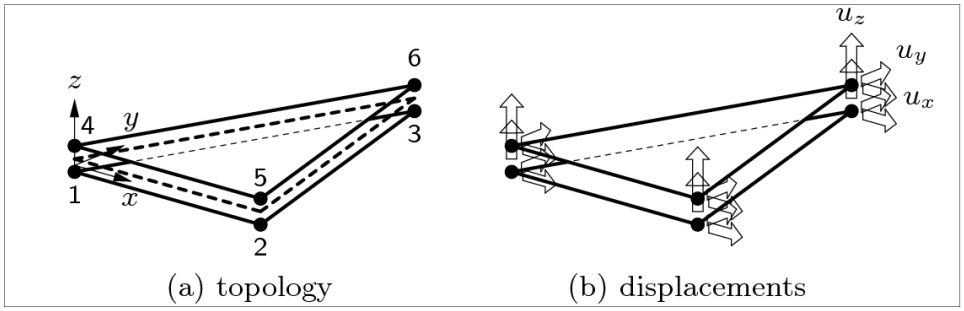

Figure 5-4 typology and displacements of plane triangular T18IF interface elements (Diana User's Manual, 2016).

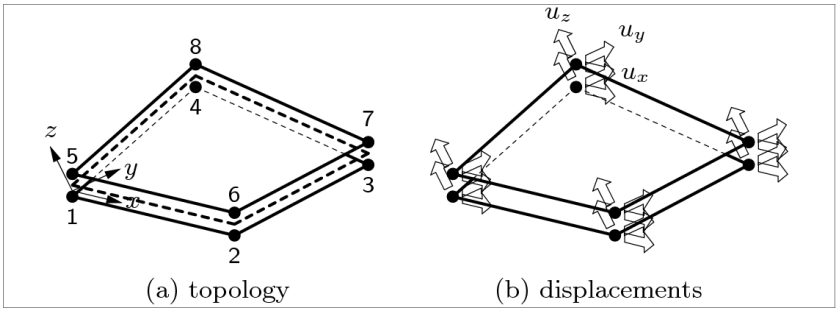

Figure 5-5 typology and displacement of plane quadrilateral Q24IF interface elements (Diana User's Manual, 2016).

Spring elements

In order to allow the lifting of the footing, one-node translational spring/dashpot elements are applied at the bottom of the concrete slabs. The basic variables of this element are the translation, the elongation and the axial force.

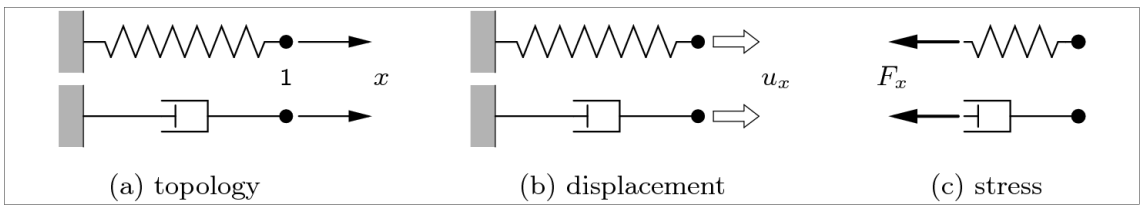

Figure 5-6 topology, displacement and stress of 1 node sp1tr spring elements (Diana User's Manual, 2016).

5.2 CONSTITUTIVE MODELS AND MATERIAL PROPERTIES

5.2.1 MASONRY

Diana offers a wide range of models to simulate the orthotropy of masonry. Meso-level approaches need to model each brick as a continuum element and joint by interfaces. For the shake of simplicity and because of the good feedbacks in previous studies, in this dissertation both arch ring and spandrel wall are modelled with a macro-model where the global behaviour is simulated.

Total Strain crack model

To model the brittle behaviour of masonry and its different strength resistance in tension and compression, the Total Strain crack model is used. This model follows a smeared approach governed by the fracture energy and evaluates the principal stresses and strains through a uniaxial stress-strain curve (Selby, R., and Vecchio, F, 1993).

For the Total Strain crack model Diana offers the options of a Rotating crack, a fixed crack, or a Rotating to fixed crack model (Diana User's Manual, 2016).

The Rotating crack model needs the maximum tensile and compressive principal strains parameters and is an efficient model for situations where crack strains are relative small. However, results are not realistic when field stress orientations change, because crack orientations are not fixed in the material.

For the Fixed crack model, in addition to the maximum tensile and compressive principal strains, the crack orientation is saved as status parameter. The crack orientation is defined as the direction of the maximum principal strain at the first moment the tensile strength is reached.

The Rotating to Fixed model is a combination of both previous models. When the critical crack strain has been reached, the crack orientation is fixed and the model changes from Rotating to Fixed model.

In this work all models used the rotating crack model because it provides better stability in the non-linear analysis (Pereira R., 2015).

Tensile and compressive behaviour

For the Total Strain crack model Diana offers different approaches based on fracture energy. In the present work a predefined linear softening functions is used. Tensile strength f_t and Mode-I tensile fracture energy G_f^I are the inputs required.

As it can be seen in Figure **5-7**, the parabolic function was chosen to model the compressive behaviour of masonry. This curve is described by three characteristic values: the strain at which one-third of the maximum compressive strength is reached, the strain at which the maximum compressive strength is reached and finally the ultimate strain.

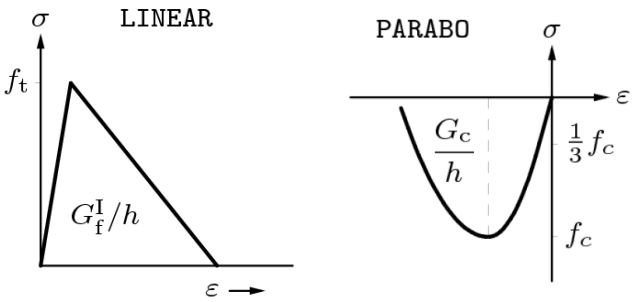

Figure 5-7 tensile and compressive functions adopted (Diana User's Manual, 2016).

In both functions the fracture energy G and the characteristic element length h govern the softening part of the curves.

5.2.2 CONCRETE AND STEEL

The slabs and the load block element are modelled with the same type of concrete with linear elastic isotropic material. Also, the steel of the plate vertical profiles and the ties have linear elastic isotropic properties.

Despite the wide range of material models that Diana offers, for the shake of simplicity and knowing that concrete and steel will not reach their ultimate strength, this simple model is a good approach in this case.

5.2.3 SOIL

Following the filling and compacting process of the experimental test, in order to have a good approach of the soil behaviour up to 5 soil layers are modelled with different Young's modulus.

A linear relationship between the Young's modulus E and the depth z is assumed:

$$\mathrm{E(z)} = \mathrm{E_0} + (\mathrm{z} - \mathrm{z_0})\frac{\partial \mathrm{E}}{\partial \mathrm{z}}$$

Where $\mathrm{E_0}$ is the Young's modulus at the soil surface, z is the vertical coordinate of the soil, $\mathrm{z_0}$ is the vertical coordinate of the soil surface and $\frac{\partial \mathrm{E}}{\partial \mathrm{z}}$ is the gradient of the Young's modulus in the vertical direction assumed as 0.32. In this formula z is given in cm and E in N/mm^2 (See Giorgia Giardina, 2015 and Salas J., 1975 in references).

Mohr – Coulomb plasticity model is used when permanent, or irreversible deformations can be observed. In the context of small strains, the strain is decomposed into an elastic part and an irreversible part: $\varepsilon = \varepsilon_e + \varepsilon_p$. The yield condition, which specifies the state of stress at which the plastic flow is initiated, in this model can be written as a function of the stress vector σ and the internal state parameter κ.

$$\mathrm{f}(\sigma, \kappa) = \frac{1}{2}(\sigma_1 - \sigma_3) + \frac{1}{2}(\sigma_1 + \sigma_3)\sin \emptyset(\kappa) - \bar{\mathrm{c}}(\kappa)\cos \emptyset_0$$

Where $\bar{c}$ is the cohesion and $\emptyset$ the internal friction angle (Diana User's Manual, 2016). If the value of the yield function is less than zero, the state is assumed to be elastic and no plastic flow will occur.

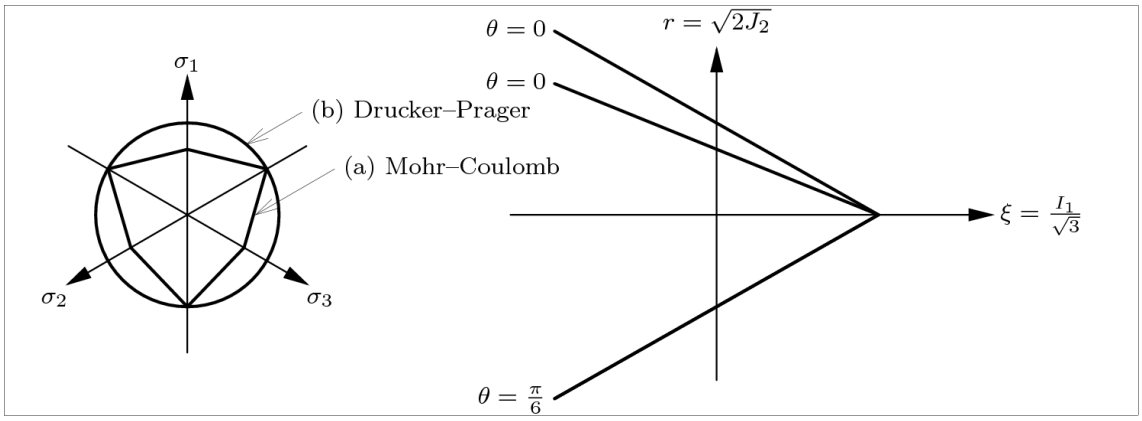

Figure 5-8 Mohr-Coulomb and Drucker-Prager yield condition (Diana User's Manual, 2016).

In order to increase the compressive strength of the infill the strain hardening hypothesis is used by applying a $\bar{c}$-κ relation. Friction and dilatancy angle are kept constant.

Also the tension cut-off value p_t is set to zero reducing the regular Mohr-Coulomb failure surface as shown in Figure **5-9**.

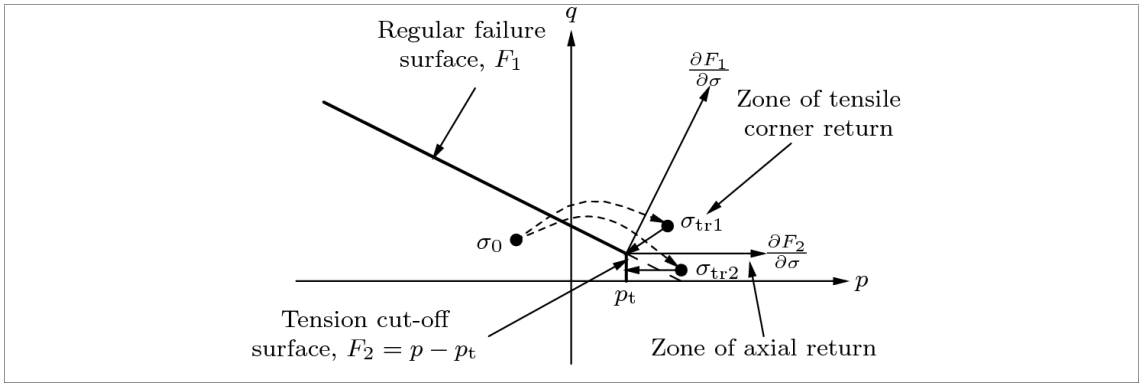

Figure 5-9 tension cut-off surface for Mohr-Coulomb plasticity model (Diana User's Manual, 2016).

5.2.4 INTERFACES

To model geometric discontinuities and the interaction between elements, two types of structural interfaces are considered. These elements relate the forces acting on the interface to the relative displacement of two sides of the interface.

- *Non-linear interface behaviour*: Combined cracking-shearing-crushing model is applied at the interfaces of the spandrel wall to simulate fracture, frictional slip and crushing along the arch ring and concrete slabs. This model was formulated by Lourenço & Rots (1997) and it is based on multi-surface plasticity, comprising a Coulomb friction model combined with a tension cut-off. It is worth to note that no three-dimensional compression cap is implemented in Diana 10.0.

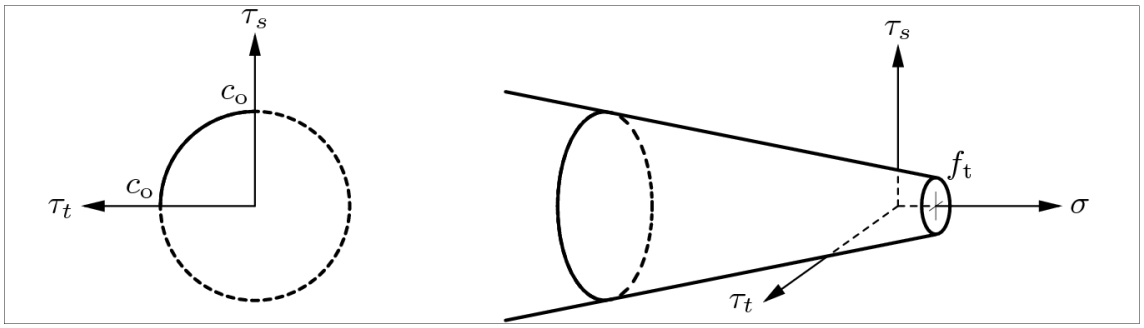

Figure 5-10 three-dimensional interface yield function (Diana User's Manual, 2016).

- *Linear interface behaviour*. Lineal stiffness model is used for the interface elements between the steel plates and the solid elements of infill, spandrel wall and concrete slabs. The reason to use a simple linear model instead of the complex cracking-shearing-crushing model was to reduce the computational time and make the analysis more stable. This linear model only needs the input of the normal and shear stiffness parameters.

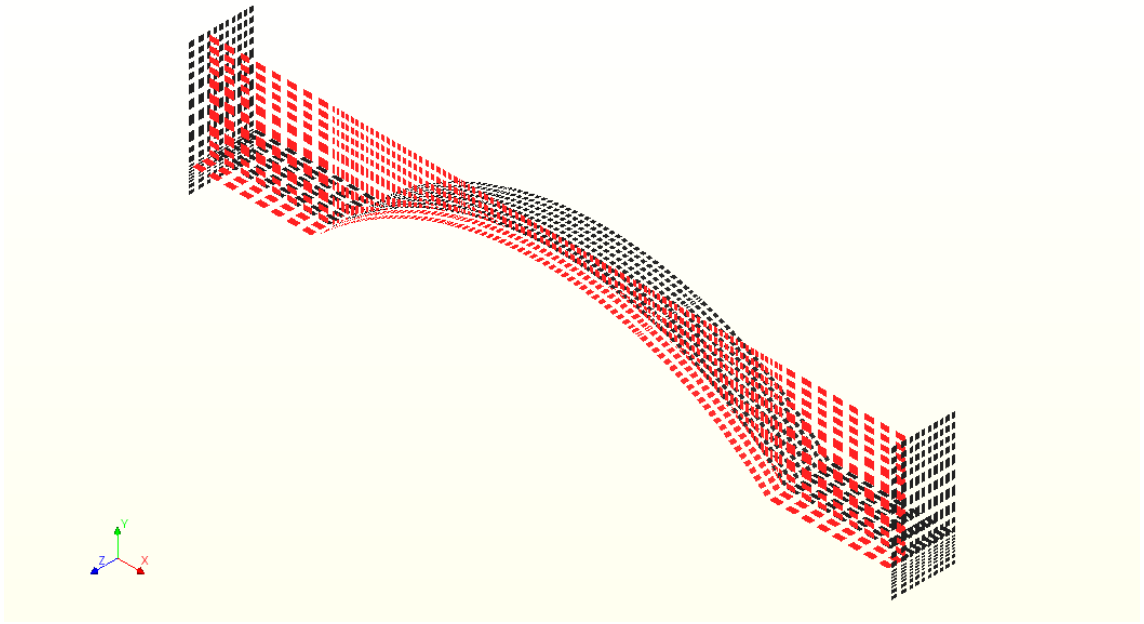

Figure 5-11 both non-linear (red) and linear (black) interface elements used in the 3D model.

To choice reasonable values of shear (K_t) and normal (K_n) stiffness of interface elements the following guidelines were used from Diana support asked questions recommendations:

$$K_n = \frac{E}{l_e} \quad , \quad K_t = \frac{K_n}{\alpha}$$

With l_e as the average element size in the mesh, E average elastic modulus between the elements surrounding the interface and α as a parameter with values from 10 to 100.

However, in some cases, the values get it from that guideline were changed by trial and error in order to avoid overlapping of the materials.

5.2.5 SPRINGS

To model unidirectional spring elements with infinite stiffness in compression and zero stiffness in tension the geometrically nonlinear tool has to be activated in the analysis window of Diana. The plasticity model is specified by ultimate forces. The maximum admissible force above which yielding occurs is set to 0 N to allow the lifting of the buttresses observed during the experimental test.

Concrete	Young's modulus	E=34000N/mm^2
	Density	2.2E-09 T/mm^3
	Poisson's ratio	0.15
Steel	Young's modulus	200000 N/mm^2
	Density	7.85E-09T/mm^3
	Poisson's ratio	0.27
Masonry	Young's modulus	5120 N/mm^2
	Density	1.8E-09 T/mm^3
	Poisson's ratio	0.18
	Tensile strength	ft=0.1 N/mm^2
	Mode-I tensile fracture energy	GfI=0.03 N/mm
	Compressive strength	fc=21 N/mm^2
	Compressive fracture energy	Gc=50 N/mm
Soil	Reference Young's modulus	15 N/mm^2
	Density	1.84E-09T/mm^3
	Poisson's ratio	0.2
	Mohr-Coulomb plasticity	
	Cohesion	0.003 N/mm^3
	Friction angle	38º
	Dilatancy angle	0º
	Tension cut-off	0 N/mm^2

Table 7 material properties for: concrete, steel, masonry and soil.

Interfaces

Linear material properties			
	Normal stiffness (N/mm^3)	Shear Stiffness (N/mm^3)	
Foots - sand	301.96	6.04	
Foots - wall	345.86	6.92	
Ring - sand	44.38	0.89	
Ring - wall	88.28	1.77	
Wall - sand	44.38	0.89	
Cover - wall	1768.28	35.37	
Cover - foots	2025.86	40.52	
Cover - sand	1724.38	34.49	
Cracking parameters			
	Tensile strength (N/mm^2)	Fracture energy (N/mm)	
Foots - wall	0.1	0.018	
Ring -wall	0.1	0.018	
Wall - sand	0.1	0.005	
Shearing parameters			
	Cohesion (N/mm^2)	Friction angle	Dilatancy angle
Foots - wall	0.05	44º	44º
Ring -wall	0.05	44º	44º
Wall - sand	0.01	44º	44º
Crushing parameters			
	Compressive strength (N/mm^2)		Factor Cs
Foots - wall	10.5		9
Ring -wall	10.5		9
Wall - sand	100		9

Table 8 material properties for interfaces.

5.3 LOAD AND BOUNDARY CONDITIONS IMPLEMENTATION

Following the recommendations of previous works (See chapter 4), for the application of the load a concrete beam of cross section 20x20cm^2 is modelled on the top of the filling and at ¼ of the arch span.

Also, to improve the convergence of the analysis, the load is applied as displacement control instead of load control. The analysis is composed for two phases:

- Phase I:
    - Structural nonlinear analysis: here only self-weight is considered. Automatic load steps size is used in order to ensure that 100% of the load is applied.
- Phase II:
    - Structural nonlinear analysis:
        - Start step load is used in order to take into account the load of the previous phase (self-weight).
        - Control displacement load is applied at the concrete beam. In the most accurate analysis steps of 0.5 mm are used until the collapse of the structure.

Another modification is made with regards to previous 3D models. Despite of using interface elements, the elements of the concrete beam in contact with the spandrel wall were removed (Figure **5-12**). As a result, the analysis has more stability and it is ensured that the load is only applied to the infill.

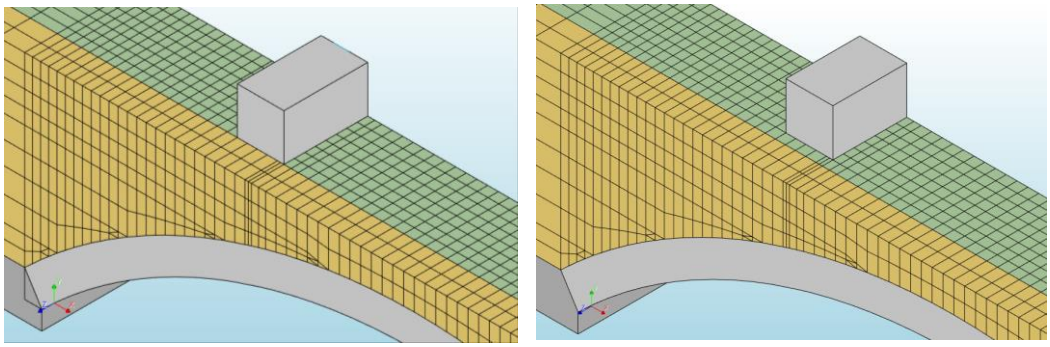

Figure 5-12 detail of the concrete beam. previous (left) and new (right) model.

The geometrical and load symmetry is taken into account. Therefore, only half of the bridge is modelled reducing the computational cost. The applied loads should be multiplied by two to take into account the other half of the bridge not modelled.

The boundary conditions applied are as follows:

- Vertical constraints at the load block beam. This constraint is only applied in Phase II of the analysis because it is necessary to use the control displacement mode.
- Horizontal constraints at the concrete slabs. Two configurations are modelled (See Figure **5-16**.
- Symmetry constraints. All the elements at the plane of symmetry have the displacement constrained at the width direction of the bridge.

- Rotation constraints at the plates. Also due to symmetry the rotation at of the plate elements at the plane of symmetry is constrained.

It is worth to note that the spring element with infinite stiffness in compression avoid the settlement of the bridge.

5.4 REPRESENTATIVE RESULTS

5.4.1 MECHANISM OF FAILURE AND DEFORMED GEOMETRY

Figure 5-13 depicts tension stress and deformed geometry observed in a section of the arch ring at the plane of symmetry. From the results, it can be seen that stresses are concentrated mainly in four areas where the hinges are expected to develop. From the beginning, tension is present at the intrados of the arch at the region under the load. After some loading steps, tensile strength of masonry is reached also at middle span, left and right springing.

It is worth to note that from figure (a) to (d) there is a reduction in tension at the region under load despite of increasing the applied load. This result can be because of the formation of some cracks between the spandrel wall and ring observed making both structural elements work independently at that area.

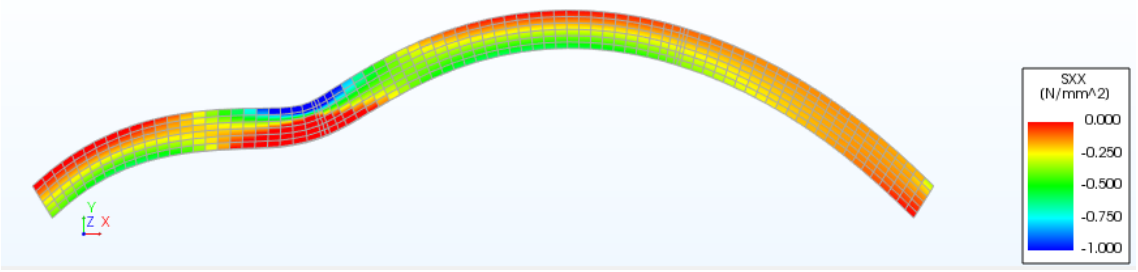

(a)

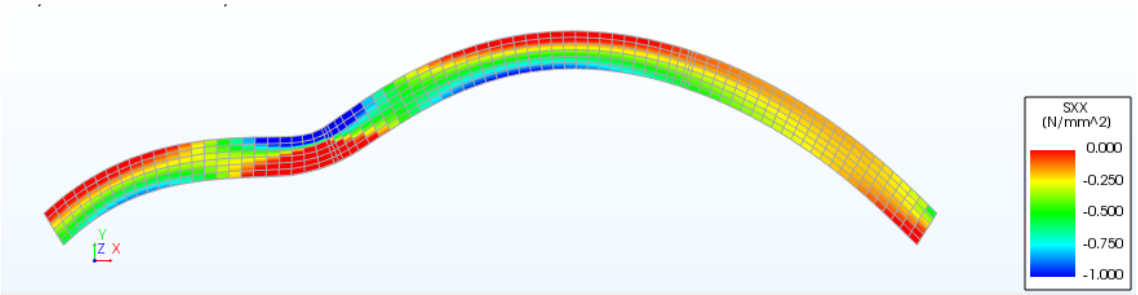

(b)

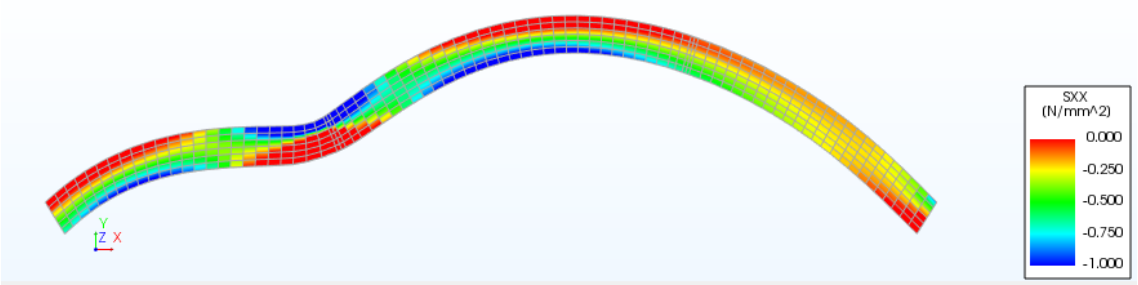

(c)

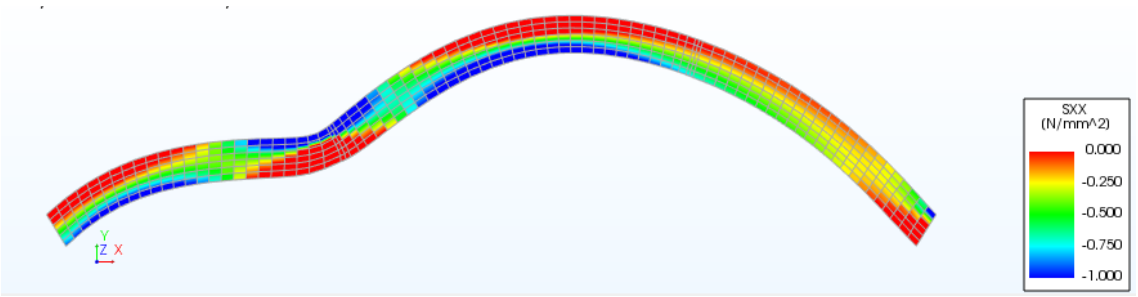

(d)

Figure 5-13 stress s_{xx} and deformed mesh of the arch ring: a 3.39 tons, b) 5.00 tons, c) 5.43 tons and d) 5.59 tons.

Certainly, interface surface elements allow simulating fracture and frictional slip at masonry elements. Masonry reaches their ultimate tensile strength at the loading region in both arch and spandrel wall. This leads to slipping and formation of the separating cracks between both elements.

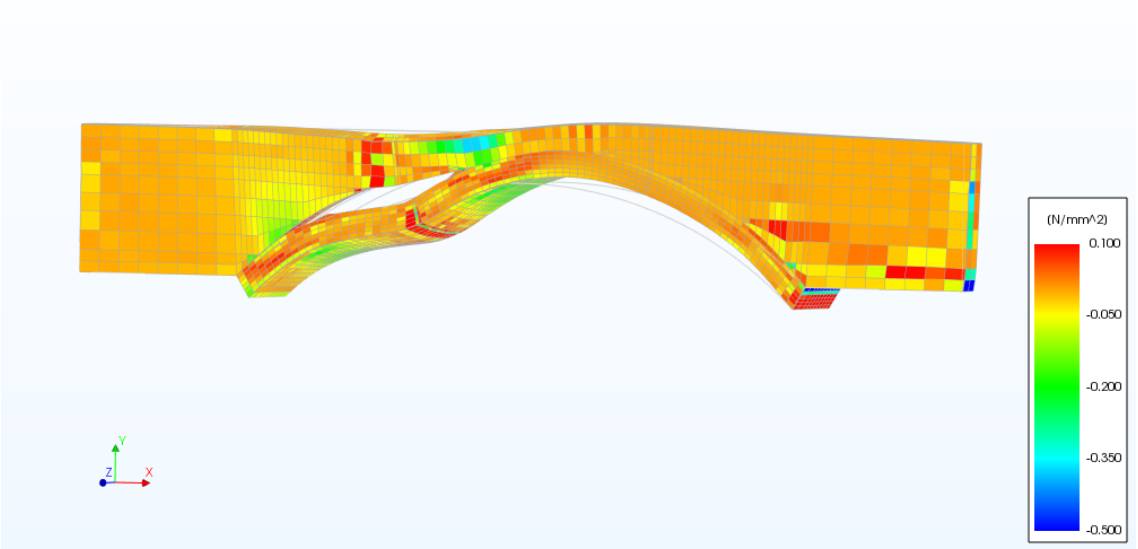

Figure 5-14 principal stress and deformed shape of the arch and spandrel wall.

The contribution of the spandrel walls for the ultimate strength is quite important due to the limited width of the bridge. Apart of retaining the infill, they limit the movement of the arch for

service loads. However, when the live load is high the arch is separated from the walls and as stated before the elements work independently.

Figure 5-15 depicts a slice of the ring in the symmetric loading region. It is possible to see that the elements at the top suffer much less tensile stress because of the longitudinal stiffness of the walls.

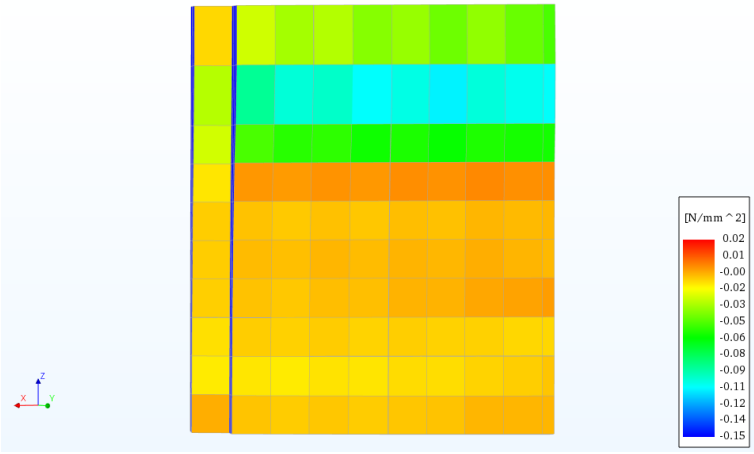

Figure 5-15 ring slice at the symmetric loading region.

The 3D model was able to reproduce the vertical displacements at the intrados of the arch which are compared with the ones from the extensiometers. These displacements are analysed for two types of support conditions. Figure **5-16** depicts the two support conditions implemented from a front view. Model (a) has one horizontal constrain along the interior wedge of the footing, and model (b) has two horizontal constrains, one at each footing.

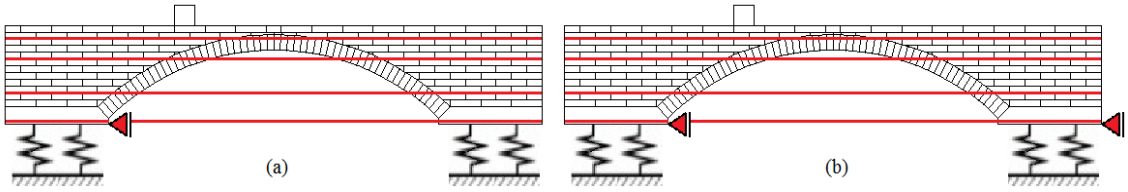

Figure 5-16 support conditions for model (a) and (b).

As expected, the area under the loaded point suffers large vertical displacement in comparison with the other two points recorded. The results of both models follow the same movement behaviours of the test: loaded point goes downwards, middle span first goes downwards and after upwards, and ¾ of span goes upwards since the beginning.

Comparing both models, the results achieved from Model (a) have very good agreement with the experimental data. The elastic behaviour where the deformations are low is almost perfect at the loaded point and ¾ of span for loads up to 3.5 tons. However, the displacement at middle span is better modelled with Model (b).

The ultimate applied load of the two models is quite similar to the one of the experimental test. However, both models are more rigid and cannot simulate the large displacements recorded in the plastic region.

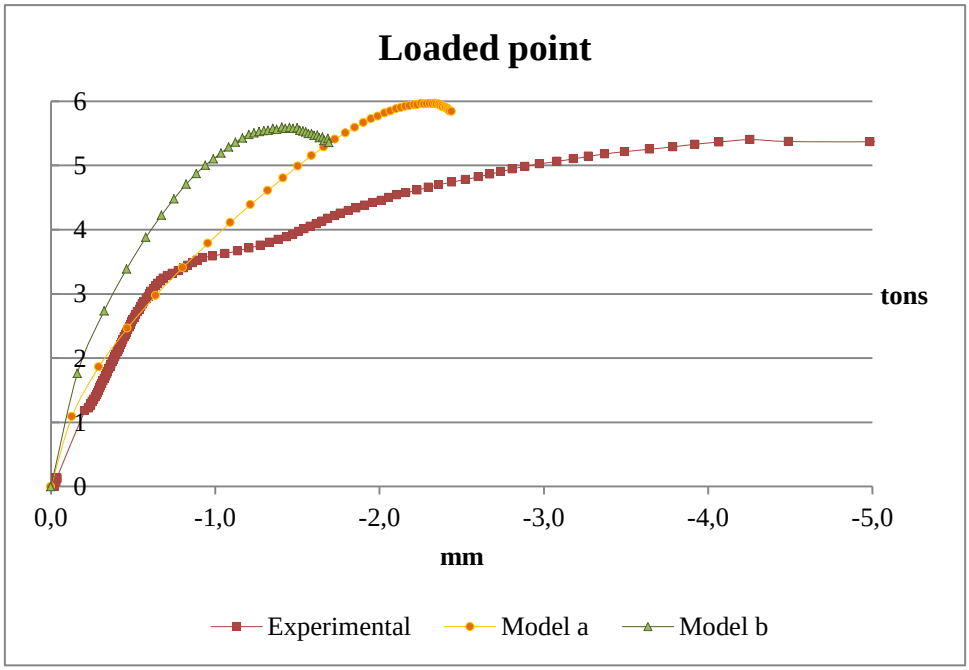

Figure 5-17 displacement at loaded point.

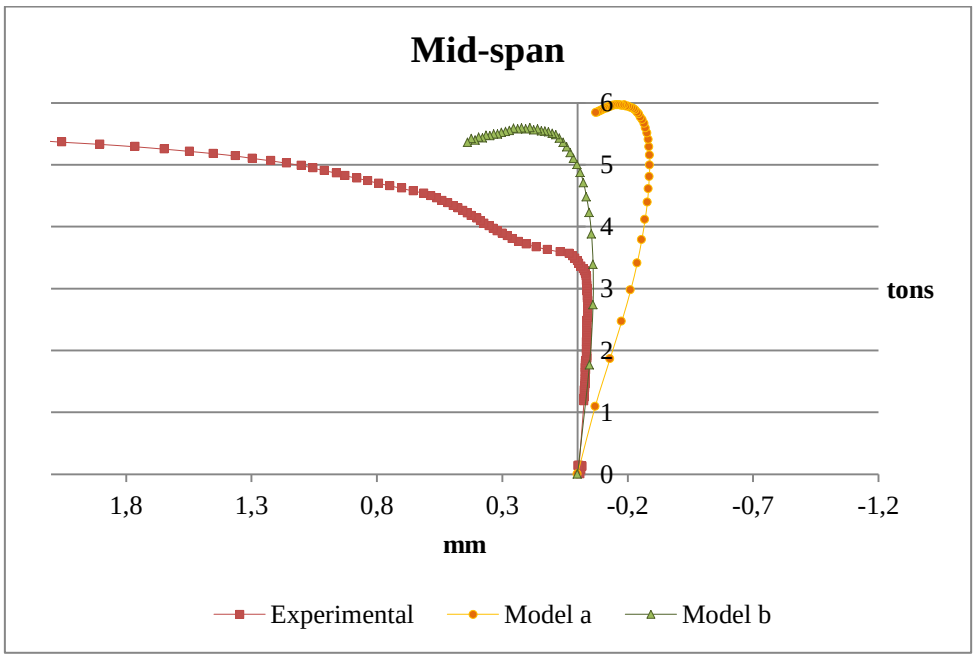

Figure 5-18 displacement at mid-span.

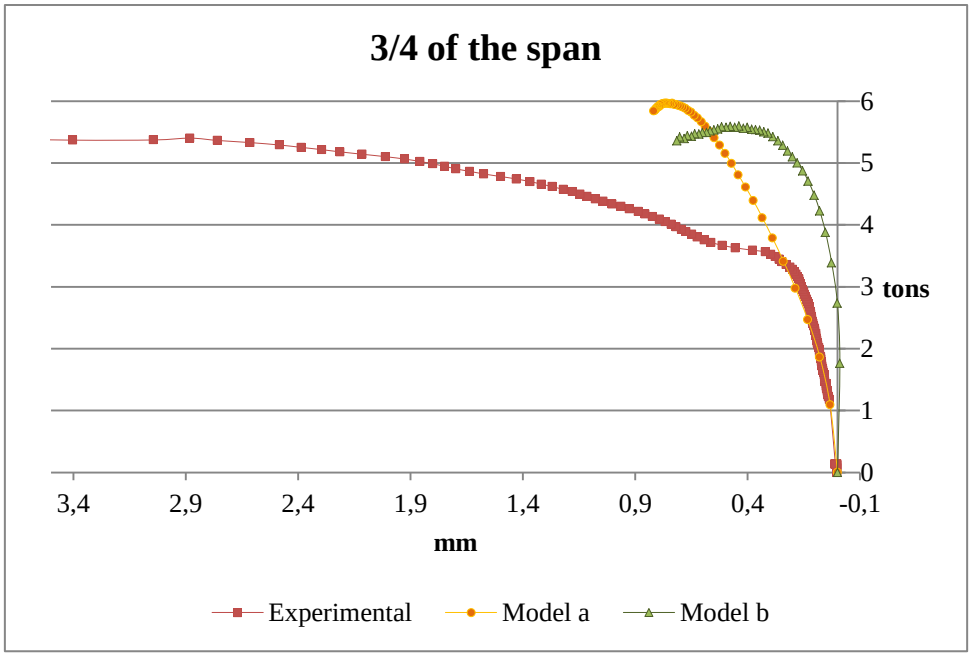

Figure 5-19 displacement at ¾ of span

In the plots, negative values mean that the movement is in the same direction of the live load whereas positive values mean the opposite direction.

5.4.2 INFLUENCE OF SOME PARAMETERS - DISPLACEMENT PLOTS

The influence of masonry tensile strength, cohesion and frictional angle of the infill is analysed. In all the plots of Figure 5-20, the soil is modelled following the Mohr-Coulomb plasticity model without hardening and applying the constrains of Model (a) (see Figure 5-16).

From the plot (a) it is concluded that increasing the tensile strength of the masonry makes the bridge stiffer in the elastic domain. However, the ultimate load is not very much different.

Plots (b) and (c) show the importance of the infill for the ultimate load of the bridge. As expected, high values of cohesion and friction angle increase the bearing capacity and the stiffness. For example, only by increasing the friction angle from 36º to 38º the ultimate load is 0.5 tons higher.

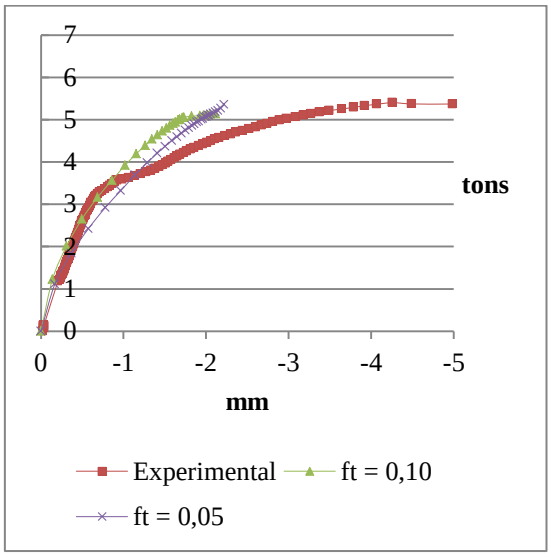

(a)

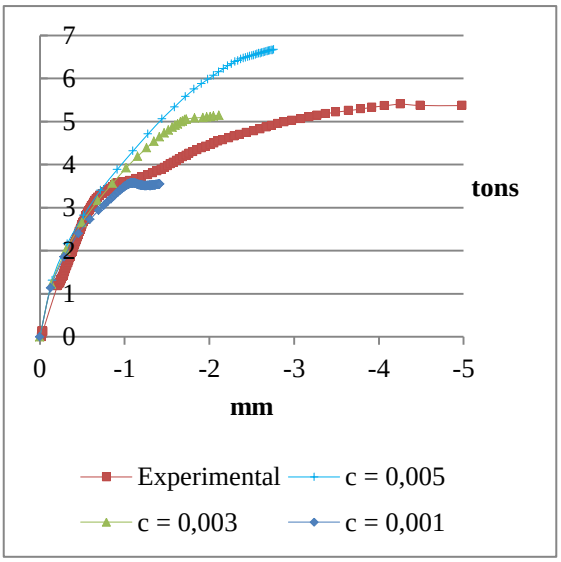

(b)

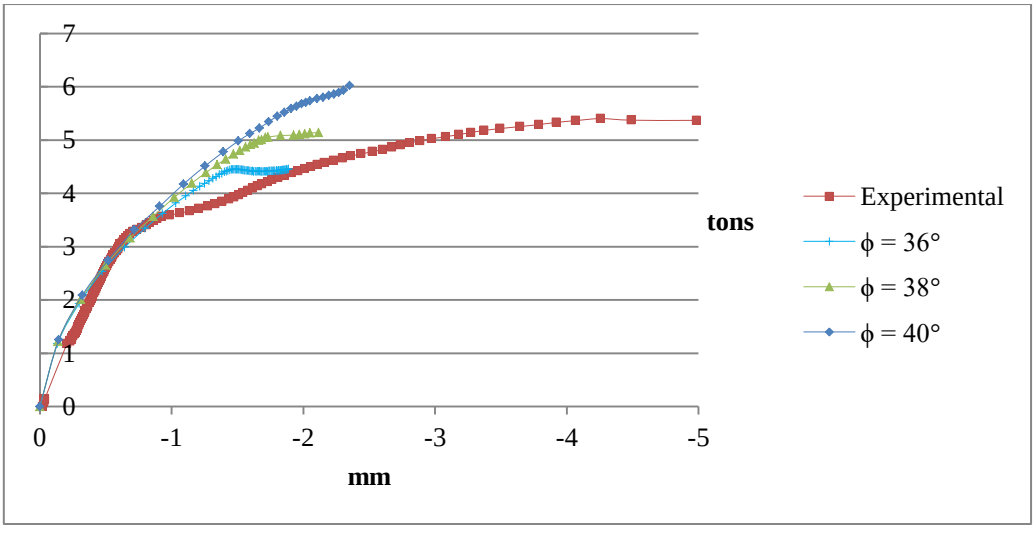

(c)

Figure 5-20 displacement plots under the loading point. Sensitive analysis of (a) masonry tensile strength, (b) cohesion of sand and (c) friction angle of sand.

5.4.3 LOAD IN THE TIES

The force on each tie is analysed for the two types of supports presented in Figure 5-16.

From the experimental data of Figure **5-21** it can be noticed that the upper tie is the one that takes the smallest part of the total horizontal thrust of the arch whereas the second, third and fourth tie have an increase of axial load quite similar up to 7 kN.

The results for Models (a) and (b) are quite different. As expected, Model (a) leads to higher load increments in all ties. This can be related to the friction of the concrete slabs with the floor providing additional horizontal thrust as in the experimental data.

It can be concluded that Model (a) gives a good approach with similar development of forces. In this model all ties have higher load increment than the experimental case for the same applied load. However, the ties in Model (b) do not behave as in the real case since the horizontal constraints bear most of the part of the thrust force. In this case, only the upper-tie gets good results because it is less influenced by the constraints in the footings.

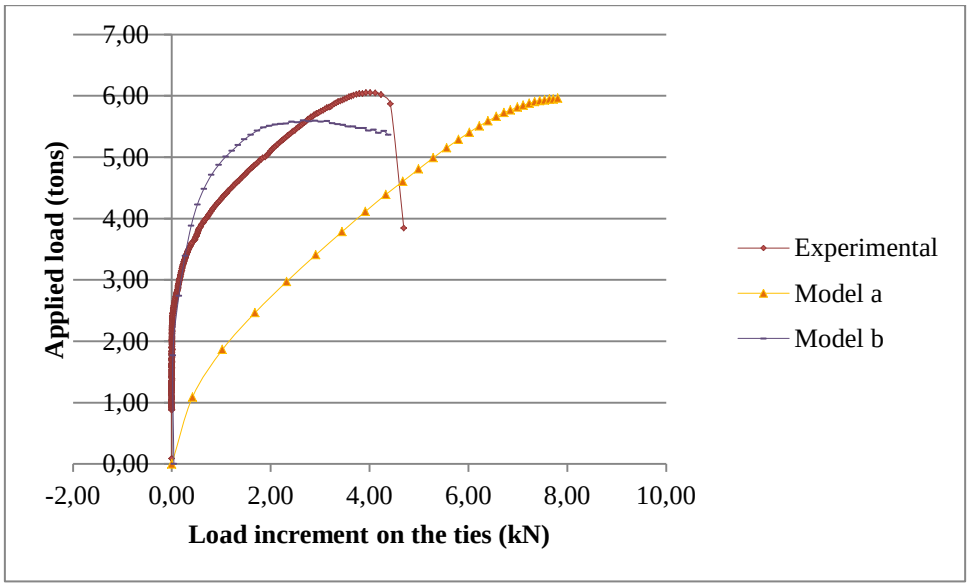

Figure 5-21 load behaviour in upper-tie 1.

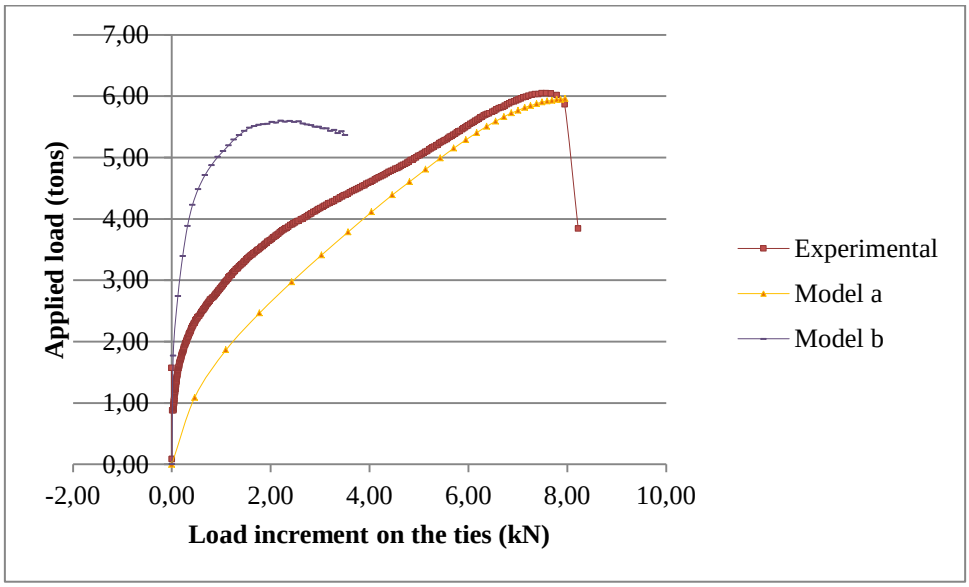

Figure 5-22 load behaviour in tie 2.

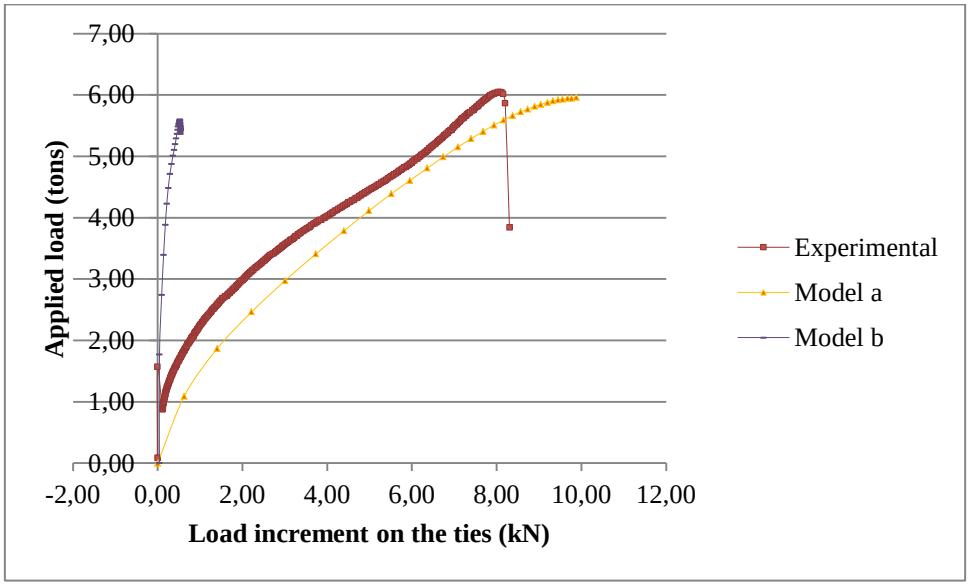

Figure 5-23 load behaviour in tie 3.

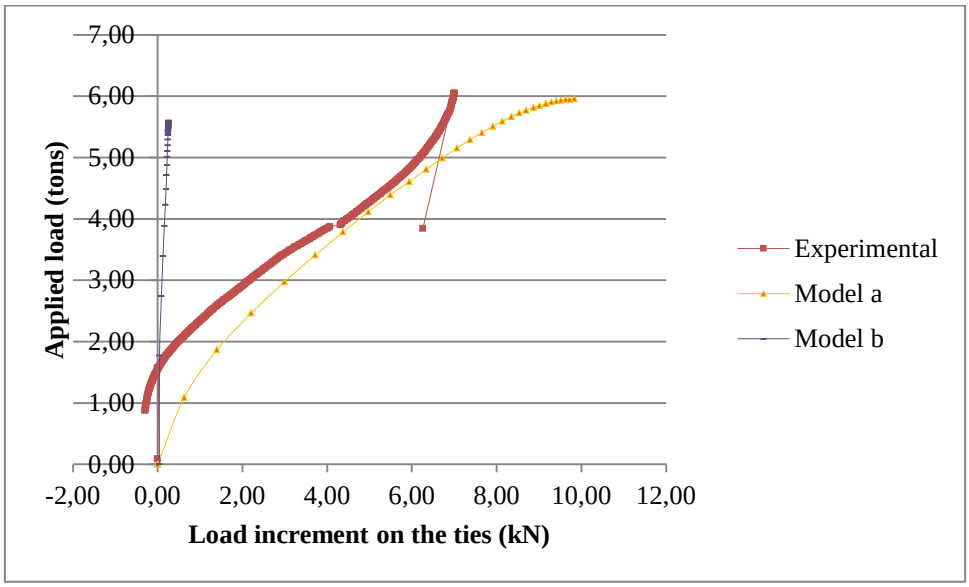

Figure 5-24 load behaviour in tie 4.

5.4.4 LIFTING OF THE BUTTRESS

The strain considerations of continuum elements used in the mesh model only work for the Enhanced Assumed Strain (EAS). However, the use of unidirectional spring elements needs the activation of geometrically nonlinear analysis.

Unfortunately, there is not option that will allow EAS to go together with geometrically nonlinear analysis. Therefore, the implementation of unidirectional spring elements was not possible and spring elements only work with linear elasticity.

For this reason, was difficult to assess the lifting of the buttress and the rotation of the slabs. Figure 5-25 depicts the observed rotation during the experimental test.

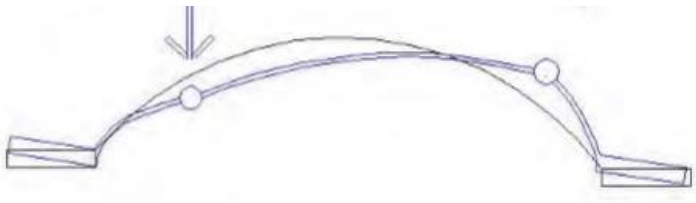

Figure 5-25 Rotation of the concrete slabs during the experiment (Serna, J., 2001).

Despite of the use of springs with high stiffness, from the results it is possible to see the parts of the bridge that go upwards. Colour red from Figure 5-26 show the vertical displacement of Model (a) with very low values but in the expected regions of the bridge.

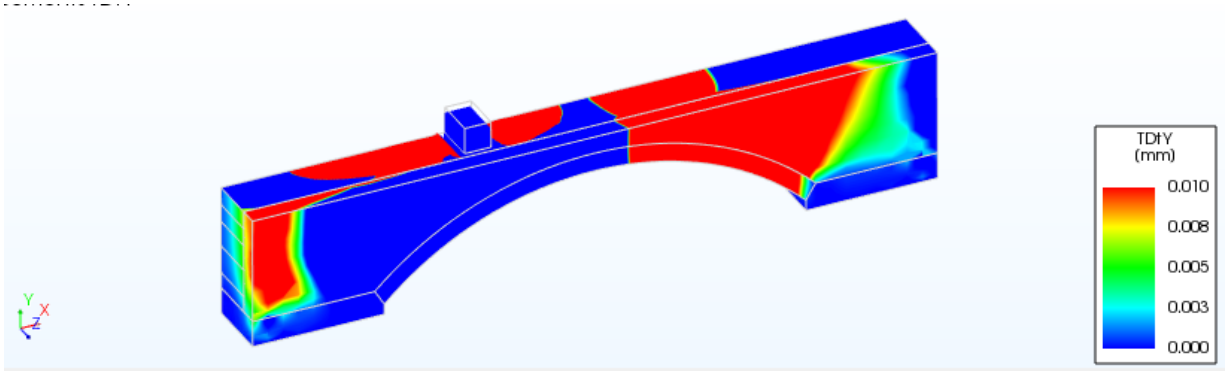

Figure 5-26 model (a) – vertical displacement.

6 CONCLUSIONS

The case of study was analysed in a 3D model approach providing very good agreement with experimental data in regard to estimate crack patterns, failure mechanism, ultimate load bearing capacity of the structure, as well as to give an insight into the overall ductility and local deformation.

Despite the procedure being complex and time consuming, this study shows the necessity to use a 3D model to represent the interaction of both infill and spandrel walls. The three dimensional behaviour is present when the soil press vertically downwards and generate a component of horizontal force carried by the spandrel walls. This transversal thrust is beneficial to the stability of the arch confining the soil. Contrary to 2D models, both spandrels and infill are present in the 3D discretization.

The understandings of the experimental test in the lab together with a thorough review of previous works provide very useful information to fix the new approach.

6.1 CONCLUSION ON THE 3D MODEL

The displacements provided by the present numerical approach have the same general behaviour at the three points under the arch ring. However, the models had a rigid behaviour and was difficult to reach large displacements in the plastic domain. The deformation of the arch and the mechanism of failure were as expected. The arch needs 4 hinges to develop a mechanism and collapse.

The use of three-dimensional surface interfaces allowed modelling the infill interaction properly. In particular, it could be seen that spandrel walls were involved in the failure mechanism and that the separation of both spandrel wall and arch was possible to simulate.

The sensitive analysis highlighted the importance of selecting the appropriate material properties. The results showed that the reduction of the tensile strength in masonry leads to less overall stiffness in the elastic region. Regarding the infill, the cohesion and friction angle were evaluated and it is stated that they have a big influence in the bearing capacity of the structure. As expected, high values of cohesion and friction angle increase the bearing capacity and the stiffness.

The presence of pre-existing crack patterns in the masonry elements was not taken into account since a macro-model approach was used. Nevertheless, masonry is approached with independent modelling of tension and compression behaviour giving realistic results in terms of strains and stresses. Micro-models are more complex but can lead to more realistic results modelling cracks between brick units.

The non-linear analysis is performed in two phases. In Phase I the use of automatic step size is needed to correctly consider the self-weight load whereas in Phase II, small load steps of 0.5mm displacement control are implemented to have reliable results. Because of the high computational time, in some cases preliminary analysis were run with larger displacement control steps.

Another improvement under study by the author was the implementation of hardening soil models. Due to the lack of information of the infill, the Modified Mohr-Coulomb model was very difficult to implement. Therefore, the Mohr-Coulomb plasticity model with strain hardening hypothesis was used allowing going further in the plastic region. This model allows increasing or decreasing the cohesion when plastic strains are present. Also, the use of tension cut-off parameter improved the works made in previous thesis.

Moreover, the load in the ties was analysed. In all ties, the increment load of the model was a bit higher but the general behaviour was in agreement with experimental data. From the results, it is possible to see which boundary conditions are the most suitable.

Finally, the lifting of the buttress was not possible to simulate because eight-node brick elements use the Enhanced Assumed Strain (EAS) which cannot be used in combination with Total Lagrange geometrical nonlinear analysis. And the use of unidirectional spring elements needs the activation of geometrical nonlinear properties. In the models, although the base remains fixed, the vertical displacements results show that there is a tendency to lift the spandrel wall in the expected areas.

6.2 SUGGESTION FOR FURTHER RESEARCH

- It is needed to have a thoroughly understanding of the parameters of the interfaces. It would be interesting to make a sensitive analysis to know how much can lead to different results.
- Implementation of a micromodel for masonry elements. This will originate more cracks and large displacements making the structure less stiff compared to reality.
- Implementation of other soil models like the Modified Mohr-Coulomb or Hardening Soil Model available in Diana software and recommended to model frictional materials like sand. Despite its complexity, the improvement of the soil model can lead to more accurate results.
- Use quadratic elements which do not require EAS and consequently no conflict with geometrically nonlinear analysis. Therefore, unidirectional spring elements may be modelled and hopefully the results will end up in larger displacements in the plastic domain. Together with the soil model, boundary conditions have proved to be very important in the general behaviour of the structure. No tension springs are needed to simulate the friction with the ground and the lifting of the buttress.

7 REFERENCES

Cai, Y., "Detailed numerical stimulation of experiments on masonry arch bridge using 3D", M.Sc. Thesis, UPC, Barcelona, 2011.

Diana – 10.0 User's Manual. Material Library 2016 by TNO DIANA BV.

Espejo Niño S. R., "Estudio del comportamiento experimental de dos puentes de fábrica ensayados hasta rotura", Trabajo de investigación tutelado ETSICCP – Universidad Politécnica de Madrid, 2007.

Forrest, B., "Simulation of Masonry Arch Experimentation Using 3D Finite Element Analysis", M.Sc. Thesis, UPC, Barcelona, 2012.

Giorgia Giardina, Matthew J., DeJong, Robert J. Mair, Tunnelling and Underground Space Technology, Department of Engineering, University of Cambridge, UK, 2015.

González, J., "Aplicación de modelos numéricos avanzados a puentes arco de obra de fábrica", M.Sc. Thesis, UPC, Barcelona, 2006.

Gutierrez, H., "Caracterización de la contribución mecánico-resistente del relleno en puentes arco de obra de fábrica", Universitat Politécnica de Catalunya, 2001.

Hoeckman, W., "Steel bridges", Faculty of Engineering of Vrije Universiteit Brussel, Academic year 2012-2013.

Huerta, S., "Mechanics of masonry vaults: the equilibrium approach", Guimarães (Portugal), 2001.

IRICEN-Indian Railways Institute of Civil Engineering, "Inspection, assessment, repairs and retrofitting of masonry arch bridges", March 2009.

Kwooi-Hock NG BEng (Hons), "Analysis of masonry arch bridges", School of the Built Environment Napier University Edinburgh, UK 1999.

Labuz, J. F., Zang, A., "Mohr-Coulomb Failure Criterion", Rock Mech Rock Eng,3 July 2012.

Lourenço, B., "Computational strategies for masonry structures: multi-scale modelling, dynamics, engineering applications and other challenges," Congreso de Métodos Numéricos en Ingeniería, Bilbao, Spain, 25-28 junio 2013.

Lourenço, B., "Computational strategies for masonry structures", Technische Universiteit Delft, 1996.

Lourenço, P. B., and Rots, J. G.A multi-surface interface model for the analysis of masonry structures. *J. Struct. Eng., ASCE 123*, 7 (1997), 660-668.

McKibbins, L.; Melbourne, C.; Sawar, N. and Sicilia Gaillard, C., "Masonry arch bridges: condition appraisal and remedial treatment", British Library Cataloguing in Publication Data, London, 2006.

Molins, C., Roca, P., Arnau, O. and Pereira, R., “Numerical simulation of experiments on masonry arch bridges”, in ARCH’16, Wroclaw, 2016.

Pereira, R., “Numerical modelling of experimental masonry arch bridge”, M.Sc. Thesis, UPC, Barcelona, 2015.

R. Farina, “Numerical modelling of experimental masonry arch bridge”, M.Sc. Thesis, UPC, Barcelona, 2015.

R. Farina, “Numerical modelling of experimental masonry arch bridge”, M.Sc. Thesis, UPC, Barcelona, 2015.

Rivera, J. E., “Puentes de fábrica y hormigón armado”, Madrid, 1925-1932.

Roca, P. and Molins, C., "Experiments on Arch Bridges", in ARCH´04, Barcelona, 2004.

Salas J. and Alpañes J., Geotecnia y Cimientos, Madrid: Editorial Rueda, 1975.

Selby, R., and Vecchio, F. “Three-dimensional Constitutive Relations for Reinforced Concrete”. Tech. Rep. 93-02, Univ. Toronto, dept. Civil Eng., Toronto, Canada, 1993

Serna, J., “Caracterización experimental del comportamiento hasta rotura de puentes en arco de obra de fábrica”, Tesina de especialidad, UPC, Barcelona, October 2001.

Tralli, A., Alessandri C. and Milani G., "Computational methods for masonry vaults: A review of recent results," The Open Civil Engeneering Journal, vol. 8, pp. 272-287, 2004.

Tralli, A., Alessandri, C. and Milani, G., "Computational methods for masonry vaults: A review of recent results", The Open Civil Engeneering Journal, vol. 8, pp. 272-287, 2004.

Vasconcelos, G. and Lourenço, P. B., “Assessment of the in-plane shear strength of stone masonry walls by simplified models,” 5th International Conference of Structural Analysis of Historical Construction, New Delhi, 2006.

Yanf Yan, B.E., M.I.R.Aust., “Progressive failure analysis of masonry arch bridges”, The university of Wollongong, New South Wales, Australia, May, 1991.